

Surface polariton excitation and energy losses by a charged particle in cylindrical waveguides

A. A. Saharian^{1,2*}, L. Sh. Grigoryan¹, A. S. Kotanjyan¹,
H. F. Khachatryan¹

¹*Institute of Applied Problems in Physics NAS RA,
25 Hr. Nersessian Str., 0014 Yerevan, Armenia*

²*Department of Physics, Yerevan State University,
1 Alex Manoogian Street, 0025 Yerevan, Armenia*

June 27, 2023

Abstract

We investigate the emission of surface polaritons (SPs) by a charged particle moving inside a dielectric cylinder parallel to its axis. It is assumed that the cylinder is immersed into a homogeneous medium with negative dielectric permittivity in the spectral range under consideration. The SP modes are present for positive dielectric function of the cylinder material. In order to find the electromagnetic fields corresponding to SPs, the respective contributions to the components of the Green tensor are separated. The expressions for scalar and vector potentials and for electromagnetic field strengths are provided inside and outside the cylinder. Those fields are expressed in terms of the SP eigenmodes of the waveguide and we give detailed analysis for their properties. The SP energy fluxes through the plane perpendicular to the cylinder axis are evaluated in the interior and exterior media. The energy flux is directed towards the charge motion inside the cylinder and towards the opposite direction in the exterior region. The relativistic effects may essentially increase the radiated energy. Important features of relativistic effects include the possibility of essential increase of the radiated energy, the narrowing the confinement region of the SP fields near the cylinder surface in the exterior region, enlarging the frequency range for radiated SPs, and the decrease of the cutoff factor for radiation at small wavelengths compared with the waveguide radius. The general results are specified for the Drude dispersion in the exterior medium. By using the Green tensor we also evaluate the total energy losses of the charged particle for general case of the interior and exterior dielectric functions. The corresponding results are compared with those previously discussed in the literature. The numerical data are presented in terms of scale invariant quantities that allows to clarify the features of the SP radiation for different values of the waveguide radius.

Keywords: Surface polariton; cylindrical waveguide; energy losses

1 Introduction

The study of various aspects of generation and propagation of surface polaritons (SPs, we use the term “surface polariton” and the related terminology in the sense clarified in Ref. [1]) is an active field

*E-mail: saharian@ysu.am

of research. They present coupled excitations of the electromagnetic field and medium polarization localized near the interface between two media. SPs are generated in the spectral range where the real parts of dielectric permittivities for neighboring materials have opposite signs. The significant attention attracted by this type of surface waves is related to their remarkable properties such as the enhancement of the electromagnetic energy density, the possibility of concentrating the corresponding fields beyond the diffraction limit for light waves, and the high sensitivity to the electromagnetic characteristics of contacting materials. Further specification of the type of SP is done based on the identification of polarization mechanism in the negative-permittivity medium. An example of a polarizable system is an electron gas in metals. The respective class of surface waves is known as surface plasmon polaritons (SPPs, see, for example, Refs. [1]-[5]). Other negative-permittivity materials supporting SP type waves are ionic crystals, semiconductors and organic dielectrics. Another possibility is to use artificially constructed materials referred to as metamaterials [6]. The spectral range for SPs can be tuned by the choice of the negative-permittivity medium or by using various mechanisms for changing the number density of charge carriers. In particular, the metamaterials and doped semiconductors allow to excite SPs in terahertz and microwave frequency ranges. Another possibility is to use subwavelength microstructured interfaces. The unique properties of SPs have resulted in wide range of applications that include biosensing, surface imaging, data storage, solar cells, surface enhanced Raman spectroscopy, nanophotonics, information processing systems, medicine and so forth.

Extensive applications of SPs in various fields of science and technology motivate the development of efficient methods for excitation of that type of waves with controllable characteristics. Available techniques for coupling electromagnetic waves in free space to SPs, widely discussed in the literature [2, 3, 4, 7], include prism and grating coupling, near-field scattering excitation and tight-focus excitation. SP modes in waveguides can also be excited by using guided photonic modes from another waveguide. Another source for SPs is provided by a beam of charged particles passing through or near the interface between negative- and positive-permittivity media. In fact, the first experimental signatures for existence of SPs were obtained in measurements of electron beam energy losses of aluminum and magnesium. High quality narrow electron beams of scanning and transmission electron microscopes (SEM and TEM, respectively) provide an excellent source in plasmonic devices with sub-nanometer resolution (see [8, 10]), essentially higher than the resolutions realized with sources based on optical beams. The emission of SPs is one of the channels for energy losses by charged particles. In particular, motivated by applications in various research and technological fields, the spectral distribution of total energy losses, including channels of very different nature, has attracted a great deal of attention (for reviews see, e.g., [8, 9]). Different types of geometries for separating surface have been discussed, including planar, spherical, cylindrical geometries and structured interfaces such as gratings. The corresponding length scales vary in rather wide intervals ranging from tens of nanometers (e.g., for carbon nanotubes and fullerenes) to millimeter and centimeter sized objects like waveguides and resonators.

The energy losses of charged particles traveling parallel to the axis of a cylindrical interface have been widely discussed in the literature (see, e.g., [8], [11]-[34] and references therein), mainly within the framework of dielectric response theory. The carbon nanotubes are among the interesting realizations of the corresponding setup. The excitation of SPs in those structures by fast electrons have been studied, for example, in [35]-[39]. The corresponding results have important applications in the microscopy and spectroscopy of materials and surfaces. The study of electron energy loss spectrum provides a useful tool in investigations of features of both surface and bulk collective excitations. The interaction between charged particles and cylindrical interfaces is of utmost importance in the physics of particle accelerators. In most of the existing literature dealing with that interaction, the total energy losses have been considered which, in addition to the radiation of SPs, include other channels as well. Our main concern in the present paper is to investigate the energy fluxes of the radiated SPs and

their distribution in negative- and positive-permittivity media. The total energy losses are separately considered as well by using the Green tensor of the electromagnetic field from [40]. The corresponding results are in agreement with those for the spectral density of the energy loss probability previously considered in the literature.

The organization of the paper is as follows. In the next section, we describe the problem setup and the components of the electromagnetic Green tensor required for evaluation of fields are presented. The contributions in the components coming from SPs are explicitly separated. In Section 3, by using the expressions for the Green tensor components, formulas are derived for the scalar and vector potentials and for the electric and magnetic fields corresponding to radiated SPs. The properties of the cylinder eigenmodes for SPs are discussed. The general expressions are specified for the special case of axial motion. In Section 4 the energy fluxes through the plane perpendicular to the cylinder axis are investigated for SPs. The energy fluxes in the interior and exterior regions are evaluated separately and the corresponding numerical results are presented. Section 5 considers energy losses by a charged particle for general case of interior and exterior dielectric permittivities. A numerical example is provided for a vacuum cylindrical hole inside a Drude like material. We then present our conclusions in Section 6.

2 Problem setup and the contribution of surface polaritons to the Green tensor

Consider a point charge q moving by a constant velocity v parallel to the axis of a cylinder with dielectric permittivity ε_0 and with the radius r_c (see Figure 1). The distance of the charge trajectory from the axis will be denoted by $r_0 < r_c$ and it will be assumed that the cylinder is immersed into a homogeneous medium with dielectric permittivity ε_1 (the magnetic permeabilities for both of the cylinder and surrounding medium will be taken to be unit). In accordance with the problem symmetry we will use cylindrical coordinates (r, ϕ, z) with the axis z along the axis of the cylinder. In the present paper we are interested in the radiation from the charge in the form of SPs.

Denoting by $x = (t, \mathbf{r})$ the spacetime point, the cylindrical components of the vector potential $\mathbf{A}(x)$ are expressed in terms of the electromagnetic field Green tensor $G_{il}(x, x')$ as

$$A_i(x) = -\frac{1}{2\pi^2 c} \int d^4 x' \sum_{l=1}^3 G_{il}(x, x') j_l(x'), \quad (2.1)$$

where $x' = (t', \mathbf{r}')$ and the current density is given by the expression

$$j_l(x) = \delta_{3l} \frac{qv}{r} \delta(\mathbf{r} - \mathbf{r}_0(t)), \quad (2.2)$$

where $\mathbf{r}_0(t) = (r = r_0, \phi = 0, z = vt)$ determines the location of the charge.

For the Green tensor we use the partial Fourier expansion

$$G_{il}(x, x') = 2\text{Re} \left[\sum_{n=-\infty}^{\infty} \int_{-\infty}^{\infty} d\omega \int_0^{\infty} dk_z G_{il,n}(\omega, k_z, r, r') e^{in\Delta\phi + ik_z\Delta z - i\omega\Delta t} \right], \quad (2.3)$$

with $\Delta\phi = \phi - \phi'$, $\Delta z = z - z'$, and $\Delta t = t - t'$. Here the relation $G_{il,-n}(-\omega, -k_z, r, r') = G_{il,n}^*(\omega, k_z, r, r')$ is used to transform the integral over the region $-\infty < k_z < +\infty$ to the integral over $0 \leq k_z < \infty$. In the problem under consideration the Fourier components $G_{i3,n}(\omega, k_z, r, r')$ are required, evaluated for $r' = r_0$. The corresponding expressions are given in [40] (for applications of the Green tensor from [40] in investigations of the Cherenkov and synchrotron radiations from a charge

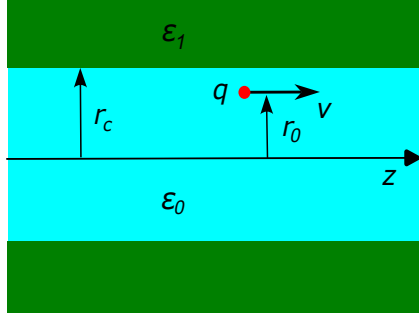


Figure 1: The problem geometry and the notations.

rotating around/inside a dielectric cylinder see [41]-[45] and references therein). They are presented in the form

$$\begin{aligned}
 G_{l3,n}(\omega, k_z, r, r_0) &= - \sum_{p=\pm 1} \frac{p^{l-1}}{i^l} C_n^{(p)} J_{n+p}(\lambda_0 r), \quad l = 1, 2, \\
 G_{33,n}(\omega, k_z, r, r_0) &= \frac{\pi}{2i} \left[J_n(\lambda_0 r_{<}) H_n(\lambda_0 r_{>}) - \frac{V_n^H}{V_n^J} J_n(\lambda_0 r_0) J_n(\lambda_0 r) \right], \quad (2.4)
 \end{aligned}$$

for the region $r < r_c$ and by

$$\begin{aligned}
 G_{l3,n}(\omega, k_z, r, r_0) &= - \sum_p \frac{p^{l-1}}{i^l} C_n^{(p)} H_{n+p}(\lambda_1 r), \quad l = 1, 2, \\
 G_{33,n}(\omega, k_z, r, r_0) &= \frac{J_n(\lambda_0 r_0)}{r_c V_n^H} H_n(\lambda_1 r), \quad (2.5)
 \end{aligned}$$

in the region $r > r_c$. Here, $l = 1, 2, 3$ correspond to the cylindrical components (r, ϕ, z) , $J_n(y)$ and $H_n(y) = H_n^{(1)}(y)$ are the Bessel and Hankel functions, $r_{<} = \min(r, r_0)$, $r_{>} = \max(r, r_0)$, and

$$V_n^F = F_n(\lambda_0 r_c) \partial_{r_c} H_n(\lambda_1 r_c) - H_n(\lambda_1 r_c) \partial_{r_c} F_n(\lambda_0 r_c), \quad (2.6)$$

with $F = J, H$, and

$$\lambda_j^2 = \omega^2 \varepsilon_j / c^2 - k_z^2, \quad j = 0, 1. \quad (2.7)$$

The coefficients in (2.4) and (2.5) are defined by the relations

$$C_n^{(p)} = \frac{k_z J_n(\lambda_0 r_0) H_n(\lambda_1 r_c)}{2 r_c \alpha_n(\omega, k_z) V_n^J V_{n+p}^J} \begin{cases} H_{n+p}(\lambda_1 r_c), & r < r_c \\ J_{n+p}(\lambda_0 r_c), & r > r_c \end{cases}, \quad (2.8)$$

where

$$\alpha_n(\omega, k_z) = \frac{\varepsilon_0}{\varepsilon_1 - \varepsilon_0} + \frac{1}{2} \sum_{l=\pm 1} \left[1 - \frac{\lambda_1 J_{n+l}(\lambda_0 r_c) H_n(\lambda_1 r_c)}{\lambda_0 J_n(\lambda_0 r_c) H_{n+l}(\lambda_1 r_c)} \right]^{-1}. \quad (2.9)$$

The equation $\alpha_n(\omega, k_z) = 0$ determines the electromagnetic eigenmodes of the cylinder. It has solutions only under the condition $\lambda_1^2 < 0$. The corresponding fields exponentially decay in the exterior medium. There are two types of the cylinder eigenmodes. For the first one, corresponding to guiding modes, we have $\lambda_0^2 > 0$ and the radial dependence of the fields inside the cylinder is given by the Bessel functions $J_n(\lambda_0 r)$ and $J_{n\pm 1}(\lambda_0 r)$. For the second type of the modes $\lambda_0^2 < 0$ and they correspond to SPs. The corresponding radial dependence inside the cylinder is expressed in terms of

the modified Bessel functions $I_n(|\lambda_0|r)$ and $I_{n\pm 1}(|\lambda_0|r)$. Here we are interested in the radiation of SPs for which $\lambda_j^2 < 0$. Introducing the modified Bessel functions, the function determining the dispersion relation is presented as

$$\alpha_n(\omega, k_z) = \frac{\varepsilon_0}{\varepsilon_1 - \varepsilon_0} + \frac{1}{2} \sum_{l=\pm 1} \left[1 + \frac{|\lambda_1| I_{n+l}(|\lambda_0|r_c) K_n(|\lambda_1|r_c)}{|\lambda_0| I_n(|\lambda_0|r_c) K_{n+l}(|\lambda_1|r_c)} \right]^{-1}. \quad (2.10)$$

From here, as a necessary condition for the presence of the roots for the equation $\alpha_n(\omega, k_z) = 0$ we get $\varepsilon_1/\varepsilon_0 < 0$. This condition requiring opposite signs for the dielectric permittivities of neighboring media is well known for planar interfaces. We will denote by $k_z = k_n(\omega)$ the positive roots of the equation $\alpha_n(\omega, k_z) = 0$. As it will be seen below, in the problem under consideration for the radiated SPs one has $\omega = k_z v$. This means that the eigenvalues of k_z for the radiated SPs are determined by the intersection of the dispersion curve $k_n(\omega)$ with the line $k_z = \omega/v$ in the (ω, k_z) -plane. In the discussion below those eigenvalues will be denoted by $k_{n,s}$, where s enumerates the roots for a given n . In the problem at hand the charge moves in the medium with permittivity ε_0 and the most promising case to escape the non-radiation energy losses and multiple scattering would be the motion in an empty cylindrical hole with $\varepsilon_0 = 1$. Motivated by this, we will specify the consideration for the case $\varepsilon_1 < 0 < \varepsilon_0$ assuming that the dielectric functions for both the media are real. The total energy losses for general complex functions $\varepsilon_0(\omega)$ and $\varepsilon_1(\omega)$ will be discussed below in Section 5. With that choice, for a given value of $\beta_0 = (v/c)\sqrt{\varepsilon_0}$, the roots with respect to

$$u = k_z r_c = \omega r_c / v, \quad (2.11)$$

are functions of the combinations $\varepsilon_1/\varepsilon_0$ and β_0 . Denoting those roots by $u_{n,s} = k_{n,s} r_c$, we get $u_{n,s} = u_{n,s}(\varepsilon_1/\varepsilon_0, \beta_0)$. In particular, they do not depend on the cylinder radius.

In the integral over k_z in (2.3) the integrand has poles at the eigenmodes of the cylinder corresponding to $\alpha_n(\omega, k_z) = 0$. The specification of the integration contour is required near those poles. In order to do that we introduce a small imaginary part for the dielectric permittivity in the exterior medium writing it in the form $\varepsilon_1 = \varepsilon_1' + i\varepsilon_1''$, where $\varepsilon_1'' = \varepsilon_1''(\omega) = \text{sgn}(\omega)|\varepsilon_1''(\omega)|$. For the function $\alpha_n(\omega, k_z)$ this gives

$$\alpha_n(\omega, k_z) \approx \alpha_n(\omega, k_z)|_{\varepsilon_1=\varepsilon_1'} + i\varepsilon_1'' \partial_{\varepsilon_1} \alpha_n(\omega, k_z)|_{\varepsilon_1=\varepsilon_1'}. \quad (2.12)$$

We have numerically checked that $\partial_{\varepsilon_1} \alpha_n(\omega, k_z)|_{\varepsilon_1=\varepsilon_1'} < 0$ for roots $k_z = k_{n,s}$. Taking the limit $\varepsilon_1'' \rightarrow 0$, it can be seen that near the poles, corresponding to the radiated SPs, the factor $1/\alpha_n(\omega, k_z)$ in the integrand for the Green tensor should be understood as $1/\alpha_n(\omega, k_z) \approx 1/[\alpha_n(\omega, k_z) - \text{sgn}(\omega)i0]$. In order to separate the respective contribution to the Green tensor we use the relation

$$\frac{1}{\alpha_n(\omega, k_z) - \text{sgn}(\omega)i0} = \mathcal{P} \frac{1}{\alpha_n(\omega, k_z)} + \text{sgn}(\omega)i\pi\delta(\alpha_n(\omega, k_z)), \quad (2.13)$$

where the symbol \mathcal{P} means that the corresponding part in the integral should be understood in the sense of the principal value.

Let us denote by $G_{il}^{(P)}(x, x')$ the part of the Green tensor coming from SPs. In addition, we will denote by $G_{il,n}^{(P)}(\omega, k_z, r, r')/\alpha_n(\omega, k_z)$ the parts in the Fourier components containing the factor $1/\alpha_n(\omega, k_z)$. Those parts only contribute to the radiation of SPs. The part $G_{il}^{(P)}(x, x')$ is determined by the contribution of the last term in (2.13) to the integral over k_z in (2.3):

$$G_{il}^{(P)}(x, x') = -2\pi \text{Im} \left[\sum_{n=-\infty}^{\infty} \sum_s \int_{-\infty}^{\infty} d\omega \text{sgn}(\omega) \frac{G_{il,n}^{(P)}(\omega, k_z, r, r')}{|\partial_{k_z} \alpha_n(\omega, k_z)|} e^{in\Delta\phi + ik_z\Delta z - i\omega\Delta t} \Big|_{k_z=k_{n,s}} \right]. \quad (2.14)$$

In particular, as it is seen from (2.4) and (2.5), $G_{33,n}^{(P)}(\omega, k_z, r, r_0) = 0$ for both the exterior and interior regions.

3 Electromagnetic fields

Having the contribution of SPs to the Green tensor we can find the related electromagnetic fields.

3.1 Vector and scalar potentials

Substituting the representation (2.14) in (2.1) and by using (2.2), for the vector potential corresponding to the radiated SPs we get

$$A_l^{(P)}(x) = \frac{2qv}{c} \text{Im} \left[\sum_{n=-\infty}^{\infty} \sum_s \frac{G_{l3,n}^{(P)}(k_z v, k_z, r, r_0)}{|\partial_{k_z} \alpha_n(\omega, k_z)|_{\omega=k_z v}} e^{in\phi + ik_z(z-vt)} \Big|_{k_z=k_{n,s}} \right]. \quad (3.1)$$

The expressions for $G_{i3,n}^{(P)}(k_z v, k_z, r, r_0)$ are obtained from (2.4) and (2.5):

$$G_{l3,n}^{(P)}(k_z v, k_z, r, r_0) = -\frac{i^{-l}}{2r_c} \sum_p^{l-1} I_n(\gamma_0 u r_0 / r_c) K_n(\gamma_1 u) \frac{R_{n+p}(u, r/r_c)}{u W_n^I W_{n+p}^I}, \quad (3.2)$$

for $l = 1, 2$, and $G_{33,n}^{(P)}(k_z v, k_z, r, r_0) = 0$. In (3.2) we use the notations (2.11) and

$$R_n(u, r/r_c) = \begin{cases} K_n(\gamma_1 u) I_n(\gamma_0 u r / r_c), & r < r_c, \\ I_n(\gamma_0 u) K_n(\gamma_1 u r / r_c), & r > r_c. \end{cases}, \quad (3.3)$$

with

$$\gamma_j = \sqrt{1 - \beta^2 \varepsilon_j}, \quad \beta = v/c, \quad (3.4)$$

and

$$W_n^I = -\gamma_1 I_n(\gamma_0 u) K_{n+1}(\gamma_1 u) - \gamma_0 I_{n+1}(\gamma_0 u) K_n(\gamma_1 u). \quad (3.5)$$

For SPs under consideration $\lambda_j = i|k_z| \gamma_j$ and the function $\alpha_n(\omega, k_z) = \alpha_n(k_z v, k_z) \equiv \alpha_n(u)$ for those modes is written in the form

$$\alpha_n(u) = \frac{\varepsilon_0}{\varepsilon_1 - \varepsilon_0} + \frac{1}{2} \sum_{l=\pm 1} \left[1 + \frac{\gamma_1 I_{n+l}(\gamma_0 u) K_n(\gamma_1 u)}{\gamma_0 I_n(\gamma_0 u) K_{n+l}(\gamma_1 u)} \right]^{-1}. \quad (3.6)$$

Note that we have assumed $\varepsilon_1 < 0 < \varepsilon_0$ and, hence, $\gamma_0 < 1 < \gamma_1$.

The insertion of (3.2) in (3.1) gives

$$A_l^{(P)}(x) = \frac{2qv}{c r_c} \sum_{n=0}^{\infty} \sum_s Q_n(u) \sum_{p=\pm 1} \frac{R_{n+p}(u, r/r_c)}{p^{l-1} u W_n^I W_{n+p}^I} \cos(u\xi/r_c) \sin(l\pi/2 - n\phi) \Big|_{u=u_{n,s}}, \quad (3.7)$$

for $l = 1, 2$, $A_3^{(P)}(x) = 0$, and the prime on the summation sign means that the term $n = 0$ should be taken with an additional coefficient 1/2. Here

$$u_{n,s} = k_{n,s} r_c, \quad \xi = vt - z, \quad (3.8)$$

and

$$Q_n(u) = \frac{K_n(\gamma_1 u)}{W_n^I \bar{\alpha}_n(u)} I_n(\gamma_0 u r_0 / r_c). \quad (3.9)$$

In (3.9) and in what follows we use the notation

$$\bar{\alpha}_n(u) = |\partial_u \alpha_n(\omega, u/r_c)|_{\omega=uv/r_c}. \quad (3.10)$$

Note that one has

$$W_{n+p}^I = -\gamma_1 I_{n+p}(\gamma_0 u) K_n(\gamma_1 u) - \gamma_0 I_n(\gamma_0 u) K_{n+p}(\gamma_1 u), \quad (3.11)$$

and the expression (3.6) for the function $\alpha_n(u)$ is rewritten in the form

$$\alpha_n(u) = \frac{\varepsilon_0}{\varepsilon_1 - \varepsilon_0} - \frac{1}{2} \gamma_0 I_n(\gamma_0 u) \sum_{p=\pm 1} \frac{K_{n+p}(\gamma_1 u)}{W_{n+p}^I}. \quad (3.12)$$

As expected, the vector potential is continuous at the cylinder surface $r = r_c$. It is important to note that, in general, the function $\bar{\alpha}_n(u)$ differs from the derivative $\alpha'_n(u)$ of the function (3.12). By using (3.11), The equation $\alpha_n(k_z v, k_z) = 0$ for SP eigenmodes $u = u_{n,s}$ is reduced to (see also [46, 47] and Ref. [48] for the corresponding guiding modes)

$$\left[\gamma_1 \frac{I'_n(\gamma_0 u)}{I_n(\gamma_0 u)} - \gamma_0 \frac{K'_n(\gamma_1 u)}{K_n(\gamma_1 u)} \right] \left[\varepsilon_0 \gamma_1 \frac{I'_n(\gamma_0 u)}{I_n(\gamma_0 u)} - \varepsilon_1 \gamma_0 \frac{K'_n(\gamma_1 u)}{K_n(\gamma_1 u)} \right] = \left(\frac{n\beta \varepsilon_0 - \varepsilon_1}{u \gamma_0 \gamma_1} \right)^2, \quad (3.13)$$

where the prime stands for the derivative of functions with respect to the argument.

The spectral component of the scalar potential $\varphi^{(P)}(x)$, denoted here as $\varphi_\omega^{(P)}$, with $\omega = u_{n,s} v / r_c$ and $\varphi_\omega^{(P)} = \int_{-\infty}^{\infty} dt \varphi^{(P)}(x) e^{i\omega t} / 2\pi$, is found by using the relation $\varphi_\omega^{(P)} = -(ic/\omega\varepsilon) \nabla \cdot \mathbf{A}_\omega^{(P)}$ in separate regions $r > r_c$ and $r < r_c$. This gives

$$\varphi^{(P)}(x) = -\frac{2q}{r_c} \sum_{n=0}^{\infty} \sum_s Q_n(u) \sum_{p=\pm 1} \frac{R_{p,n}^{(e)}(u, r/r_c)}{u W_{n+p}^I} \sin(u\xi/r_c) \cos(n\phi) |_{u=u_{n,s}}, \quad (3.14)$$

with the notation

$$R_{p,n}^{(e)}(u, r/r_c) = \begin{cases} \frac{\gamma_0}{\varepsilon_0} K_{n+p}(\gamma_1 u) I_n(\gamma_0 u r/r_c), & r < r_c \\ -\frac{\gamma_1}{\varepsilon_1} I_{n+p}(\gamma_0 u) K_n(\gamma_1 u r/r_c), & r > r_c \end{cases}. \quad (3.15)$$

We can check that the spectral components of the scalar potential obey the boundary condition

$$\varepsilon_0 \partial_r \varphi_\omega^{(P)} |_{r=r_c-0} - \varepsilon_1 \partial_r \varphi_\omega^{(P)} |_{r=r_c+0} = i(\varepsilon_0 - \varepsilon_1) \frac{\omega}{c} A_{\omega 1}^{(P)} |_{r=r_c}, \quad (3.16)$$

where the expression for the spectral component of the vector potential on the cylinder surface directly follows from (3.7).

It is important to mention that the potentials $\varphi^{(P)}(x)$ and $\mathbf{A}^{(P)}(x)$ are the parts of the total fields corresponding to radiated SPs. The total fields can be found by using the relation (2.1) and the components (2.4) and (2.5) for the electromagnetic field Green tensor. The part in the fields coming from the first term in the square brackets of the expression (2.4) for the component $G_{33,n}(\omega, k_z, r, r_0)$ corresponds to the field generated by a charged particle moving in a homogeneous medium with dielectric permittivity ε_0 . Denoting by $\mathbf{A}^{(0)}(x) = (0, 0, A_3^{(0)}(x))$ the corresponding vector potential, we get

$$A_3^{(0)}(x) = -\frac{qv}{2ic} \int_{-\infty}^{\infty} dk_z e^{ik_z(z-vt)} \sum_{n=-\infty}^{\infty} e^{in\phi} J_n(\lambda_0 r_<) H_n(\lambda_0 r_>). \quad (3.17)$$

The series over n in this expression is summed by using the addition theorem for the cylinder functions (see, for example, [49]). By taking into account that $\lambda_0 = ik_z \gamma_0$, the sum of the series is equal to $2K_0(k_z \gamma_0 r_\perp) / (\pi i)$, where $r_\perp = \sqrt{r^2 + r_0^2 - 2rr_0 \cos \phi}$ is the distance of the observation point (r, ϕ, z) from the trajectory of the charge. For the spectral component of the vector potential, $A_{\omega 3}^{(0)}$, this gives $A_{\omega 3}^{(0)} = q e^{i\frac{\omega}{v} z} K_0(\frac{\omega}{v} \gamma_0 b) / (\pi c)$. The corresponding scalar potential is obtained from the relation $\varphi_\omega^{(0)} = -(ic/\omega\varepsilon_0) \partial_z A_{\omega 3}^{(0)}$ and one gets $\varphi_\omega^{(0)} = A_{\omega 3}^{(0)} / (\beta\varepsilon_0)$. The spectral component of the electric field

strength is found by using the formula $\mathbf{E}_\omega^{(0)} = i\omega\mathbf{A}_\omega^{(0)}/c - \nabla\varphi_\omega^{(0)}$. In particular, for the z -projection we find

$$E_{\omega 3}^{(0)} = -\frac{iq\omega}{\pi v^2} \left(\frac{1}{\varepsilon_0} - \beta^2 \right) e^{i\frac{\omega}{v}z} K_0\left(\frac{\omega}{v}\gamma_0 r_\perp\right). \quad (3.18)$$

For $z = 0$ this result differs from the corresponding expression given in Ref. [48] (see Eq. (13.32)) by an additional coefficient $1/\sqrt{2\pi}$ which is related to different coefficients in the definition of the Fourier transformation.

3.2 Magnetic and electric fields

The cylindrical components of the magnetic field \mathbf{H} are found from the relation $\mathbf{H} = \nabla \times \mathbf{A}$. Denoting the part related to SPs by $\mathbf{H}^{(P)}$ and by making use of the recurrence relations for the modified Bessel functions one obtains

$$\begin{aligned} H_l^{(P)}(x) &= \sum_{n=0}^{\infty} \sum_s H_{l,n}^{(P)}(u_{n,s}) \sin(u_{n,s}\xi/r_c) \cos(\pi l/2 - n\phi), \\ H_3^{(P)}(x) &= \sum_{n=0}^{\infty} \sum_s H_{3,n}^{(P)}(u_{n,s}) \cos(u_{n,s}\xi/r_c) \sin(n\phi), \end{aligned} \quad (3.19)$$

where

$$\begin{aligned} H_{l,n}^{(P)}(u) &= -2\delta_n \frac{q\beta}{r_c^2} Q_n(u) \sum_{p=\pm 1} \frac{R_{n+p}(u, r/r_c)}{p^l W_{n+p}^I}, \\ H_{3,n}^{(P)}(u) &= 2\delta_n \frac{q\beta}{r_c^2} Q_n(u) \sum_{p=\pm 1} \frac{R_{p,n}^{(m)}(u, r/r_c)}{p W_{n+p}^I}, \end{aligned} \quad (3.20)$$

and $\delta_0 = 1/2$, $\delta_n = 1$ for $n > 1$. In (3.20) we have defined the function

$$R_{p,n}^{(m)}(u, r/r_c) = \begin{cases} \gamma_0 K_{n+p}(\gamma_1 u) I_n(\gamma_0 u r/r_c), & r < r_c \\ -\gamma_1 I_{n+p}(\gamma_0 u) K_n(\gamma_1 u r/r_c), & r > r_c \end{cases}, \quad (3.21)$$

for the exterior and interior regions. It can be checked that the magnetic field is continuous on the cylinder surface.

From the relation $\mathbf{E}_\omega = i\omega\mathbf{A}_\omega/c - \nabla\varphi_\omega$ we find the spectral components of the electric field for radiated SPs. The corresponding Fourier expansions have the form

$$\begin{aligned} E_l^{(P)}(x) &= \sum_{n=0}^{\infty} \sum_s E_{l,n}^{(P)}(u_{n,s}) \sin(u_{n,s}\xi/r_c) \sin(\pi l/2 - n\phi), \\ E_3^{(P)}(x) &= \sum_{n=0}^{\infty} \sum_s E_{3,n}^{(P)}(u_{n,s}) \cos(u_{n,s}\xi/r_c) \cos(n\phi), \end{aligned} \quad (3.22)$$

where $l = 1, 2$. The Fourier components are expressed as

$$\begin{aligned} E_{l,n}^{(P)}(u) &= \delta_n \frac{q}{r_c^2} Q_n(u) \sum_{p,p'=\pm 1} \frac{1 + pp'\beta_0^2}{p^{l-1}} \frac{K_{n+p'}(\gamma_1 u)}{\varepsilon_0 W_{n+p'}^I} I_{n+p}(\gamma_0 u r/r_c), \quad r < r_c, \\ E_{l,n}^{(P)}(u) &= \delta_n \frac{q}{r_c^2} Q_n(u) \sum_{p,p'=\pm 1} \frac{1 + pp'\beta^2 \varepsilon_1}{p^{l-1}} \frac{I_{n+p'}(\gamma_0 u)}{\varepsilon_1 W_{n+p'}^I} K_{n+p}(\gamma_1 u r/r_c), \quad r > r_c, \end{aligned} \quad (3.23)$$

and

$$E_{3,n}^{(P)}(u) = -\frac{2\delta_n q}{r_c^2} \sum_{p=\pm 1} \frac{Q_n(u)}{W_{n+p}^I} R_{p,n}^{(e)}(u, r/r_c). \quad (3.24)$$

It can be checked that the components $E_2^{(P)}(x)$ and $E_3^{(P)}(x)$ for the electric field and the component $D_1^{(P)}(x)$ for the displacement vector are continuous on the boundary $r = r_c$. The expressions for separate components can be further simplified by using the relations

$$\begin{aligned} \sum_{p=\pm 1} \frac{K_{n+p}(\gamma_1 u)}{W_{n+p}^I} &= \frac{2\varepsilon_0/(\varepsilon_1 - \varepsilon_0)}{\gamma_0 I_n(\gamma_0 u)}, \\ \sum_{p=\pm 1} \frac{I_{n+p}(\gamma_0 u)}{W_{n+p}^I} &= \frac{2\varepsilon_1/(\varepsilon_0 - \varepsilon_1)}{\gamma_1 K_n(\gamma_1 u)}, \end{aligned} \quad (3.25)$$

which directly follows from $\alpha_n(u) = 0$ in combination with (3.12). Note that both the electric and magnetic fields, in addition to the transversal components, have longitudinal components.

The expressions for the fields are further simplified on the axis of the cylinder. The cylindrical coordinates are degenerate for $r = 0$ and, in order to take the limit $r \rightarrow 0$, we first transform the fields to Cartesian coordinates (x, y, z) , where the x -axis corresponds to $\phi = 0$ and for the location of the charge one has $(x, y, z) = (r_0, 0, vt)$. In this way, for the nonzero Cartesian components of the electric and magnetic fields on the cylinder axis, $r = 0$, one finds

$$\begin{aligned} H_y^{(P)} &= \frac{2q\beta}{r_c^2} \sum_s \frac{Q_1(u)}{W_0^I} K_0(\gamma_1 u) \sin(u\xi/r_c) |_{u=u_{1,s}}, \\ E_x^{(P)} &= \frac{2q}{r_c^2} \sum_s Q_1(u) \left[\frac{\beta^2}{W_0^I} K_0(\gamma_1 u) - \frac{\gamma_0/(\varepsilon_0 - \varepsilon_1)}{I_1(\gamma_0 u)} \right] \sin(u\xi/r_c) |_{u=u_{1,s}}, \\ E_z^{(P)} &= -\frac{q}{r_c^2} \sum_s \frac{\gamma_0 Q_0(u)}{\varepsilon_0 W_1^I} K_1(\gamma_1 u) \cos(u\xi/r_c) |_{u=u_{0,s}}. \end{aligned} \quad (3.26)$$

Hence, on the axis the electric and magnetic fields are orthogonal and the magnetic field is transversal

We recall that for given β_0 and $\varepsilon_1/\varepsilon_0$ the eigenmodes $u_{n,s}$ do not depend on the cylinder radius r_c . The eigenvalues for the SP wavelength are expressed as $\lambda_{\text{sp}} = \lambda_{n,s} = 2\pi r_c/u_{n,s}$. The dependence of the Fourier components $E_{l,n}^{(P)}(u_{n,s})$ and $H_{l,n}^{(P)}(u_{n,s})$ on the cylinder radius appears in the form of the coefficient q/r_c^2 and in the form of the ratios r_0/r_c and r/r_c in the arguments of the modified Bessel functions. Note that the dependence on the impact parameter r_0 comes from the function $I_n(\gamma_0 u r_0/r_c)$ in the definition (3.9) for $Q_n(u)$. Hence, for fixed values of the other parameters the absolute values $|E_{l,n}^{(P)}(u_{n,s})|$ and $|H_{l,n}^{(P)}(u_{n,s})|$ monotonically increase with increasing $r_0 < r_c$. The fields in the negative-permittivity medium depend on the radial coordinate through the functions $K_n(\gamma_1 u_{n,s} r/r_c)$, $K_{n\pm 1}(\gamma_1 u_{n,s} r/r_c)$ and, hence, they are exponentially suppressed at distances $r \gg \lambda_{n,s}/(2\pi\gamma_1)$. For a given wavelength, the SP fields in the negative-permittivity medium are mainly localized near the cylinder surface within the region of the thickness $\lesssim \lambda_{n,s}/(2\pi\gamma_1)$. In the problem at hand $\gamma_1 > 1$ and the localization radius can be essentially smaller than the wavelength. Note that the parameter γ_1 increases with increasing β and the localization near the cylinder surface in the exterior region is stronger for relativistic electrons (for the discussion of relativistic effects in radiation of SPs see also [8]).

3.3 Properties of the modes

The electromagnetic fields for SPs are expressed in terms of the corresponding eigenmodes of the cylinder. In this subsection the properties of those modes are discussed. We can consider the equation

$\alpha_n(u) = 0$, with $\alpha_n(u)$ from (3.6), as an equation determining the ratio $\varepsilon_1/\varepsilon_0$ for given values u and β_0 : $\varepsilon_1/\varepsilon_0 = f_n(u, \beta_0)$. Let us clarify the asymptotic properties of the roots interpreted in that way. For large values of u , assuming that $\gamma_j u \gg 1$, by using the asymptotic expressions for the modified Bessel functions (see, for example, [49]) in (3.6) we get

$$\alpha_n(u) \approx \frac{\varepsilon_0}{\varepsilon_1 - \varepsilon_0} + \left(1 + \frac{\gamma_1}{\gamma_0}\right)^{-1} \left(1 + \frac{1}{2\gamma_0 u}\right). \quad (3.27)$$

From here it follows that in the limit $u \rightarrow \infty$ the roots of the equation $\alpha_n(u) = 0$ with respect to $\varepsilon_1/\varepsilon_0$ tend to the limiting value $1/(\beta_0^2 - 1)$. Note that to the leading order one has

$$\gamma_1/\gamma_0 \approx -\varepsilon_1/\varepsilon_0. \quad (3.28)$$

This is an exact relation in the limit of a planar boundary. By taking into account that $u = 2\pi r_c/\lambda_{\text{sp}}$, we see that the large values for u correspond to wavelengths much smaller than the cylinder radius. We could expect that in this limit the curvature effects of the separating boundary will be weak.

In the opposite limit $u \ll 1$ and for the modes with $n = 0$ one finds

$$\alpha_0(u) \approx \frac{\varepsilon_1}{\varepsilon_1 - \varepsilon_0} + \frac{1}{4}u^2\gamma_1^2 \ln(u\gamma_1). \quad (3.29)$$

This shows that for those modes the roots with respect to $\varepsilon_1/\varepsilon_0$ tend to zero. For $n \geq 1$ and $u \ll 1$ the asymptotic expressions for the function $\alpha_n(u)$ have the form

$$\begin{aligned} \alpha_1(u) &\approx \frac{1 + \varepsilon_1/\varepsilon_0}{2(\varepsilon_1/\varepsilon_0 - 1)} - \frac{\gamma_1^2 u^2}{16} - \frac{1}{4}\gamma_0^2 u^2 \ln(\gamma_1 u), \\ \alpha_n(u) &\approx \frac{1 + \varepsilon_1/\varepsilon_0}{2(\varepsilon_1/\varepsilon_0 - 1)} + u^2 \frac{2 + [(n-1)\varepsilon_1 - (n+1)\varepsilon_0]\beta^2}{8n(n^2 - 1)}, \end{aligned} \quad (3.30)$$

with $n \geq 2$ in the second line. From here we conclude that for $n \geq 1$ the roots $\varepsilon_1/\varepsilon_0$ tend to -1 .

Now let us consider the properties of SP modes for large values of n . By using the uniform asymptotic expansions of the modified Bessel function for large values of the order [49], to the leading order we get

$$\alpha_n(u) \approx \frac{\varepsilon_0}{\varepsilon_1 - \varepsilon_0} + \frac{1}{2} \sum_{l=\pm 1} \left(1 + \frac{\gamma_1^2 \sqrt{1 + u^2 \gamma_0^2/n^2} - l}{\gamma_0^2 \sqrt{1 + u^2 \gamma_1^2/n^2} + l}\right)^{-1}. \quad (3.31)$$

First let us consider the possibility of the modes with $u\gamma_j \ll n$ when the leading order term is reduced to

$$\alpha_n(u) \approx \frac{\varepsilon_1 + \varepsilon_0}{\varepsilon_1 - \varepsilon_0} + \mathcal{O}(1/n^2). \quad (3.32)$$

From here it follows that for large n the corresponding modes are present if the ratio $\varepsilon_1/\varepsilon_0$ is sufficiently close to -1 : $\varepsilon_1/\varepsilon_0 \approx -1 + \mathcal{O}(1/n^2)$. For the modes with $u\gamma_j$ of the order $n \gg 1$, solving the equation $\alpha_n(u) = 0$, with $\alpha_n(u)$ from (3.31), we get

$$u_{n,s} \approx n \left(\frac{\beta_0^2 \varepsilon_1}{\varepsilon_0 + \varepsilon_1} - 1 \right)^{-1/2}. \quad (3.33)$$

In the region under consideration the neighboring roots with respect to n are approximately equidistant.

In Figure 2 we have presented the distribution of the roots for the equation $\alpha_n(u) = 0$ with respect to $\varepsilon_1/\varepsilon_0$ as functions of u . On the left panel the graphs are plotted for $n = 0$ and $n = 1$ (the dashed and full curves respectively) and for fixed values of β_0 (the numbers near the curves). The right panel

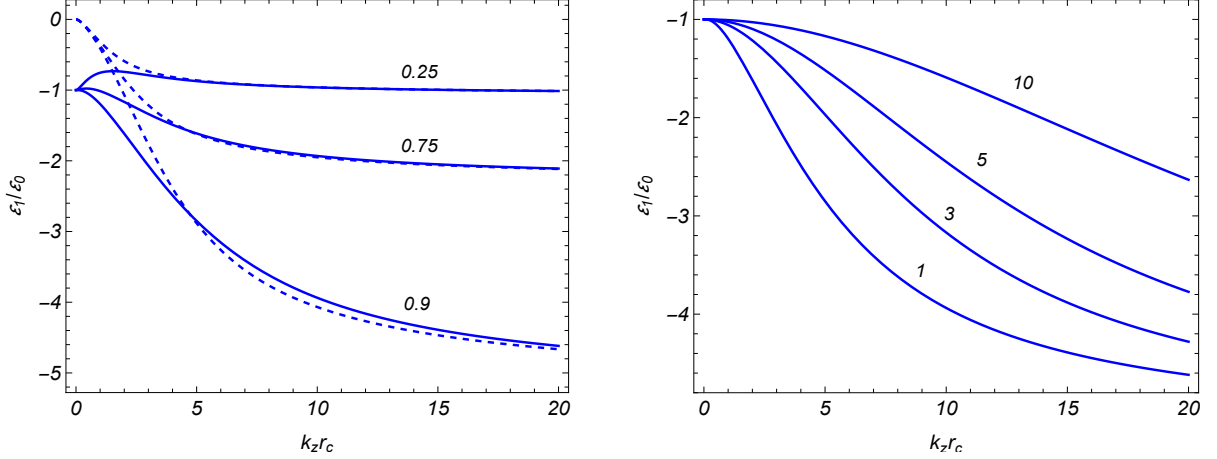


Figure 2: The roots of the eignemode equation for SPs with respect to the ratio $\varepsilon_1/\varepsilon_0$ as functions of $u = k_z r_c$. The dashed and full curves on the left panel correspond to the modes with $n = 0$ and $n = 1$, respectively, and the numbers near the curves are the values of β_0 . The right panel is plotted for $\beta_0 = 0.9$ and for different values of n (the numbers near the curves).

presents the graphs for different values of n (the numbers near the curves) and for $\beta_0 = 0.9$. The numerical data confirm the features clarified by the asymptotic analysis: $\varepsilon_1/\varepsilon_0$ tends to $-1 + \delta_{0n}$ in the limit $u \rightarrow 0$ and $\varepsilon_1/\varepsilon_0 \rightarrow 1/(\beta_0^2 - 1)$ for $u \rightarrow \infty$.

We have considered the general properties of SP modes without fixing the dispersion law for the dielectric functions $\varepsilon_j(\omega)$. Figure 2 displays the function $\varepsilon_1/\varepsilon_0 = f_n(u, \beta_0)$ for different values of β_0 and n . Given the dielectric functions $\varepsilon_j(\omega) = \varepsilon_j(uv/r_c)$, the eigenvalues for u are determined by the intersections of the graphs for the functions $\varepsilon_1(uv/r_c)/\varepsilon_0(uv/r_c)$ and $f_n(u, \beta_0)$. As an example we will consider the Drude model for the exterior medium assuming that the dispersion of the material of the cylinder in the frequency range under consideration is weak. The simplest example would be the motion of the charge in an empty cylindrical hole with $\varepsilon_0 = 1$. Denoting by ω_p and η the plasma frequency and the characteristic collision frequency, the function $\varepsilon_1 = \varepsilon_1(\omega)$ is expressed as

$$\varepsilon_1(\omega) = 1 - \frac{\omega_p^2}{\omega^2 + i\eta\omega}. \quad (3.34)$$

In accordance with the assumption made above, to clarify the qualitative features we will ignore the imaginary parts of both dielectric permittivities ε_0 and $\varepsilon_1(\omega)$. The effect of the imaginary parts on the energy losses of the charge in the problem at hand will be considered in Section 5 below. The dispersion described by (3.34) is the most popular model in theoretical considerations of SPs. Putting $\eta = 0$ in (3.34), for the upper frequency of SPs one gets $\omega < \omega_p$ and for the charge velocity we have $\beta < 1/\sqrt{\varepsilon_0}$. In terms of the variable (2.11) this constraint is reduced to $u < r_c \omega_p/v$. From the features of the distribution of the roots $u_{n,s}$, described above for general real ε_0 and ε_1 , it follows that for a given β_0 and $r_c \omega_p/c \gg 1$ for the roots corresponding to ω/ω_p one has $\omega/\omega_p \approx 1/\sqrt{1 + \varepsilon_0/\gamma_0^2}$. In the opposite limit $r_c \omega_p/c \ll 1$ the roots with respect to ω/ω_p tend to 1 for $n = 0$ and to $1/\sqrt{1 + \varepsilon_0}$ for $n \geq 1$. Again, based on the general analysis presented above, we can see that for fixed $r_c \omega_p/c$ and for large values of n one has $\varepsilon_1(\omega)/\varepsilon_0 \approx -1$ or, in terms of the angular frequency, $\omega/\omega_p \approx 1/\sqrt{1 + \varepsilon_0}$. In accordance of the interpretation given above, specified for the special case at hand, the radiation modes $u = u_{n,s}$ are determined by the intersection of the curves $\varepsilon_1 = 1 - (r_c \omega_p/v)^2/u^2$ and $f_n(u, \beta_0)$. As seen from Figure 2, for the corresponding example there is a unique solution and we can omit the index s for $u_{n,s}$ and the summation over s in the expressions for the fields given above.

In Figure 3 the roots of the eigenvalue equation for SPs with respect to the ratio ω/ω_p are depicted as functions of the combination $\omega_p r_c/c$ for the dispersion law (3.34) ignoring the absorption. For the region $r < r_c$ we have taken $\varepsilon_0 = 1$. The left panel presents the curves for the modes $n = 0$ (dashed lines) and $n = 1$ (full lines). The numbers near the curves are the values of β . The right panel displays the location of the roots for $\beta = 0.5$ and for the modes $n = 1, 2, 3, 5, 10$ (the numbers near the curves). The numerical data confirm the asymptotic analysis given above.

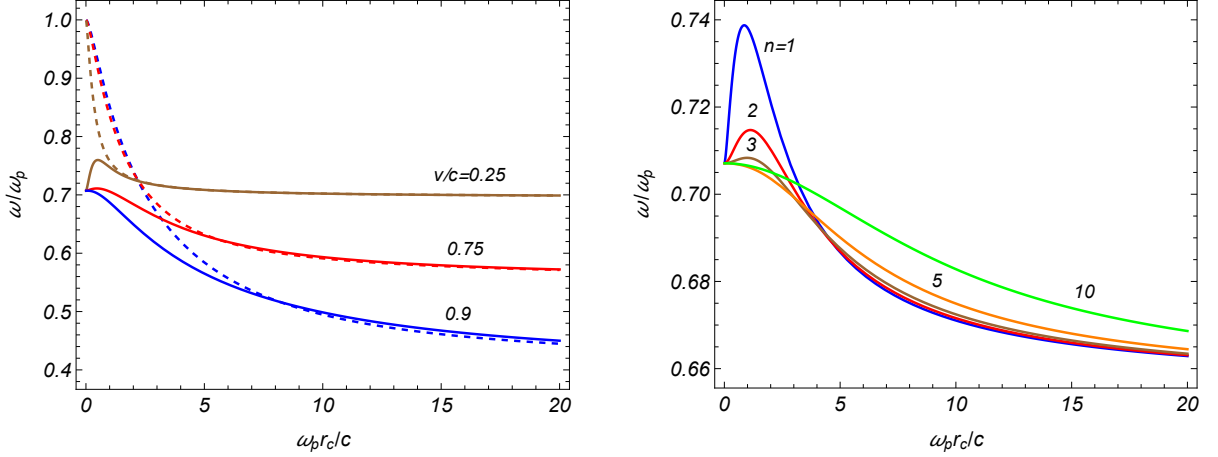


Figure 3: The frequencies of SP modes versus the combination $\omega_p r_c/c$ in the case of the Drude model of dispersion for $\varepsilon_1(\omega)$ and for $\varepsilon_0 = 1$. The dashed and full curves on the left panel correspond to the modes $n = 0$ and $n = 1$, respectively. The numbers near the curves are the corresponding values of β . The graphs on the right panel are plotted for different values of n (the numbers near the curves) and for $\beta = 0.5$.

As it has been discussed above, for large values of n we can have two qualitatively different cases for the behavior of the modes $u_{n,s}$. For given ε_0 and ε_1 , when ε_1 is not too close to $-\varepsilon_0$, the roots linearly increase with increasing n (see (3.33)). This type of the behavior for $r_0/r_c = 0.95$ is illustrated on the left panel of Figure 4. The corresponding values for the pair $(\varepsilon_1/\varepsilon_0, \beta_0)$ are presented on the figure. In the second case, the permittivity ε_1 is close to $-\varepsilon_0$ (see (3.32)) and for large n one has $u_{n,s} \ll n$. This case is realized, for example, by the dispersion law (3.34) with $\eta = 0$ and for the motion of the charge in vacuum, $\varepsilon_0 = 1$. The results of the corresponding numerical evaluations for ω/ω_p , with the values of the parameters $r_0/r_c = 0.95$, $\beta = 0.9$, are presented on the right panel of Figure 4. The numbers near the points correspond to the values of $r_c \omega_p/c$. For large n the ratio ω/ω_p tends to $1/\sqrt{2}$ (dashed line, corresponding to $1/\sqrt{1+\varepsilon_0}$ in the asymptotic analysis given above) and $\varepsilon_1(\omega)$ tends to $-\varepsilon_0 = -1$. On the right panel of Figure 4, for the $n = 0$ mode in the case $r_c \omega_p/c = 1$ one has $\omega/\omega_p \approx 0.852$. With decreasing β the distribution of the modes near the line $1/\sqrt{2}$ becomes narrower. This feature can also be seen from Figure 3.

In the non-relativistic limit, assuming that $\beta^2 |\varepsilon_j| \ll 1$, to the leading order, we can replace γ_0 and γ_1 in (3.6) by 1. The corresponding expression is simplified by using the Wronskian relation for the modified Bessel function and we get

$$\alpha_n(u) \approx \frac{\varepsilon_0}{\varepsilon_1 - \varepsilon_0} - u I_n(u) K_n'(u). \quad (3.35)$$

Hence, in the non-relativistic limit the equation determining the eigenmodes for the SPs reads

$$u I_n(u) K_n'(u) = \frac{\varepsilon_0}{\varepsilon_1 - \varepsilon_0}. \quad (3.36)$$

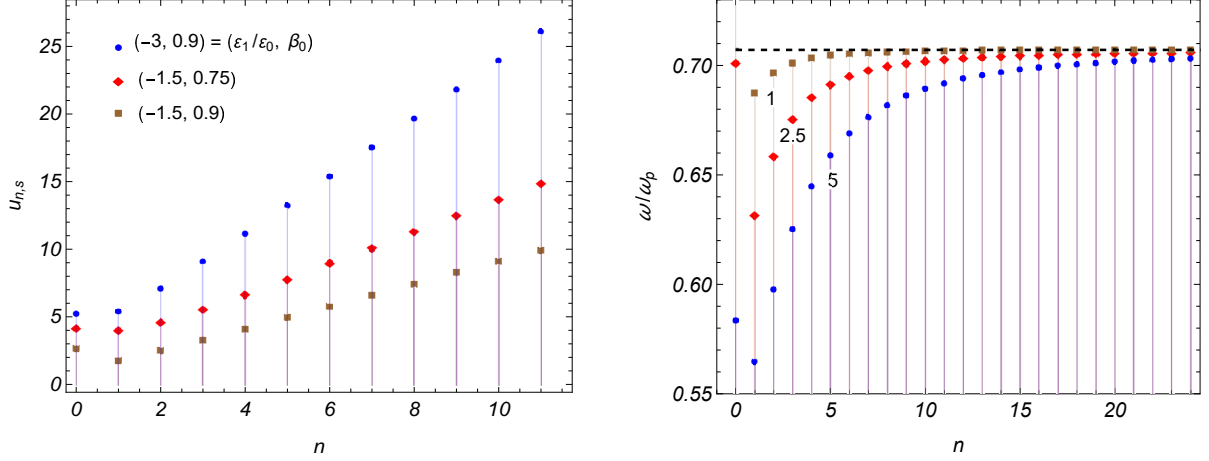


Figure 4: SP modes as functions of n for the ratio $r_0/r_c = 0.95$. The left panel presents the roots with respect to $u = k_z r_c$ for given values of the pair $(\varepsilon_1/\varepsilon_0, \beta_0)$. On the right panel the modes with respect to the ratio ω/ω_p are depicted in the Drude model (3.34) with $\eta = 0$. The numbers near the points are the values of $r_c \omega_p/c$.

This equation can also be written in the form $u I'_n(u) K_n(u) = \varepsilon_1/(\varepsilon_1 - \varepsilon_0)$. Combining these two forms we get another equivalent representation

$$\frac{\varepsilon_1}{\varepsilon_0} = \frac{I'_n(u) K_n(u)}{I_n(u) K'_n(u)}. \quad (3.37)$$

This form has been used, for example, in [21]. Similar to the interpretation given above, we can consider (3.36) as an equation that determines the ratio $\varepsilon_1/\varepsilon_0$ as a function of u for a given n : $\varepsilon_1/\varepsilon_0 = f_n(u)$. By making use of the properties of the modified Bessel functions we can see that $\lim_{u \rightarrow \infty} f_n(u) = -1$ for all n , $f_0(0) = 0$, and $f_n(0) = -1$ for $n > 0$. In addition we have $f_n(u) > f_{n+1}(u)$ and $-1 < f_n(u) < 0$ for $0 < u < \infty$. The function $f_0(u)$ is monotonically decreasing, whereas the functions $f_n(u)$ with $n > 0$ have the maximum $f_n^{(m)} < 0$, $0 \leq f_n(u) \leq f_n^{(m)}$, which decreases with increasing n . From this analysis we conclude that in the non-relativistic limit SP modes are present in the range $-1 \leq \varepsilon_1/\varepsilon_0 < 0$ for $n = 0$ and in the range $-1 \leq \varepsilon_1/\varepsilon_0 \leq f_n^{(m)}$ for $n > 0$. The allowed region for $\varepsilon_1/\varepsilon_0$ becomes narrower with increasing n . All those features are seen from the left panel of Figure 5 where we have displayed the function $\varepsilon_1/\varepsilon_0 = f_n(u)$ for different values of n (the numbers near the curves). The right panel in Figure 5 presents the dependence of the frequency of the SPs on the parameter $r_c \omega_p/v$ for the model of dispersion (3.34) (with $\eta = 0$) and for $\varepsilon_0 = 1$ in the non-relativistic limit. The numbers near the curves are the values of n . In the limit $r_c \omega_p/v \rightarrow 0$ we have $\omega/\omega_p \rightarrow 0$ for $n = 0$ and $\omega/\omega_p \rightarrow 1/\sqrt{2}$ for $n > 0$. In the opposite limit $r_c \omega_p/v \rightarrow \infty$ we get $\omega/\omega_p \rightarrow 1/\sqrt{2}$. Comparing with the data presented in Figures 2 and 3 we see that the relativistic effects may essentially enlarge the regions for $\varepsilon_1/\varepsilon_0$ in the general case and for ω/ω_p in the Drude model allowing the existence of the SP modes.

3.4 Fields for a charge moving along the cylinder axis

The expressions for the electromagnetic fields corresponding to the generated SPs are essentially simplified in the special case of the charge motion along the axis of the cylinder corresponding to $r_0 = 0$. The dependence of the fields on r_0 enters in the expressions for the fields in the form of the modified Bessel function $I_n(\gamma_0 u r_0/r_c)$ in (3.9). From here we conclude that the only nonzero contribution comes from the mode with $n = 0$ and the fields do not depend on the angular coordinate

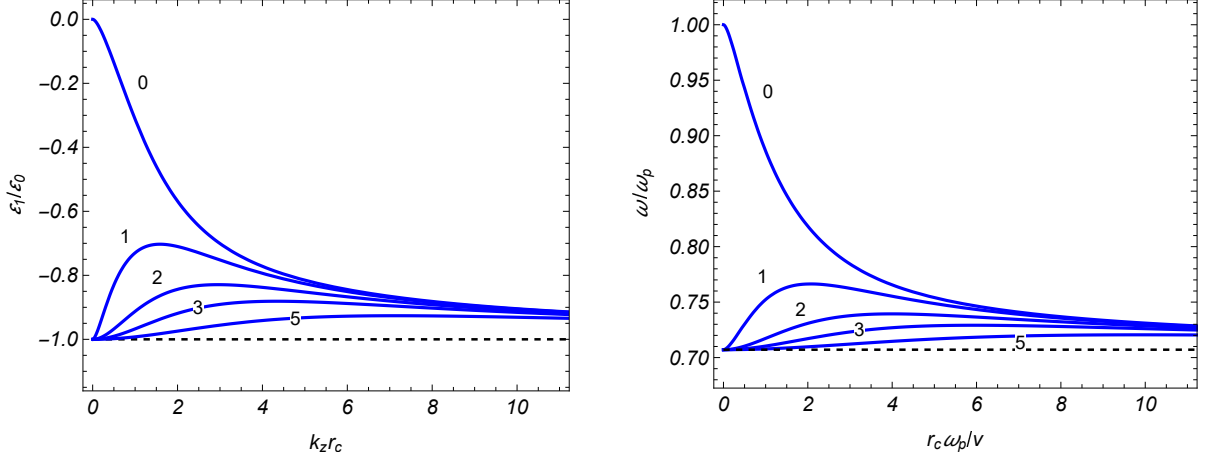


Figure 5: The left panel presents the function $\varepsilon_1/\varepsilon_0 = f_n(k_z r_c)$ for SPs in the non-relativistic limit of the charge motion. The right panel describes the dependence of the ratio ω/ω_p on the quantity $r_c \omega_p/v$ for the Drude model of dispersion in the same limit. The numbers near the curves are the corresponding values for n .

ϕ . Of course, that is a direct consequence of the problem symmetry in the special case at hand. For the function (3.12) one gets

$$\alpha_0(u) = \frac{\varepsilon_0 \gamma_1 I_1(\gamma_0 u) K_0(\gamma_1 u) + \varepsilon_1 \gamma_0 I_0(\gamma_0 u) K_1(\gamma_1 u)}{(\varepsilon_0 - \varepsilon_1) W_1^I}, \quad (3.38)$$

and the equation determining the eigenmodes for SPs take the form

$$\frac{I_1(\gamma_0 u) K_0(\gamma_1 u)}{I_0(\gamma_0 u) K_1(\gamma_1 u)} = -\frac{\varepsilon_1 \gamma_0}{\varepsilon_0 \gamma_1}. \quad (3.39)$$

In the non-relativistic limit the latter is reduced to (3.37) with $n = 0$. Note that we have $0 < \gamma_0 < 1 < \gamma_1$. Under these conditions the function in the left-hand side of (3.39) is monotonically increasing from 0 for $u = 0$ and approaching 1 in the limit $u \rightarrow \infty$. From here it follows that the SP modes are present under the condition $1/(\beta_0^2 - 1) < \varepsilon_1/\varepsilon_0 < 0$ and there is a single mode for given β_0^2 and $\varepsilon_1/\varepsilon_0$ obeying that condition.

From the general formulas, by using the equation (3.39), for the nonzero components of the potentials we get

$$\begin{aligned} \varphi^{(P)}(x) &= \frac{q}{r_c} Q(u) R_{(0)}(u, r/r_c) \sin(u\xi/r_c), \\ A_1^{(P)}(x) &= -\frac{q}{r_c} \beta \varepsilon Q(u) R_{(1)}(u, r/r_c) \cos(u\xi/r_c), \end{aligned} \quad (3.40)$$

where $\varepsilon = \varepsilon_0$ for $r < r_c$, $\varepsilon = \varepsilon_1$ for $r > r_c$, and

$$Q(u) = \frac{2\varepsilon_1 (\varepsilon_0 - \varepsilon_1)^{-2} \gamma_0}{u I_1(\gamma_0 u) \bar{\alpha}_0(u)}. \quad (3.41)$$

The dependence on the radial coordinate is expressed in terms of the functions

$$R_{(0)}(u, w) = \begin{cases} \frac{I_0(\gamma_0 u w)}{I_0(\gamma_0 u)}, & w < 1 \\ \frac{K_0(\gamma_1 u w)}{K_0(\gamma_1 u)}, & w > 1 \end{cases}, \quad (3.42)$$

and

$$R_{(1)}(u, w) = \begin{cases} \frac{I_1(\gamma_0 u w)}{\gamma_0 I_0(\gamma_0 u)}, & w < 1 \\ -\frac{K_1(\gamma_1 u w)}{\gamma_1 K_0(\gamma_1 u)}, & w > 1 \end{cases}. \quad (3.43)$$

For the nonzero components of the electric and magnetic fields one finds

$$\begin{aligned} E_1^{(P)}(x) &= \frac{H_2^{(P)}(x)}{\beta \varepsilon} = -\frac{q}{r_c^2} u Q(u) R_{(1)}(u, r/r_c) \sin(u\xi/r_c), \\ E_3^{(P)}(x) &= \frac{q}{r_c^2} u Q(u) R_{(0)}(u, r/r_c) \cos(u\xi/r_c), \end{aligned} \quad (3.44)$$

where u is a root of the equation (3.39). For the special case of axial motion the electric and magnetic fields are orthogonal and the magnetic field is transversal.

4 Energy fluxes for radiated surface polaritons

Having the expressions of the fields for radiated SPs, in this section we evaluate the energy flux through the plane perpendicular to the cylinder axis. The latter is determined by the Poynting vector and is given by

$$I^{(f)} = \frac{c}{4\pi} \int_0^{2\pi} d\phi \int_0^\infty dr r \left[\mathbf{E}^{(P)} \times \mathbf{H}^{(P)} \right] \cdot \mathbf{n}_z, \quad (4.1)$$

with \mathbf{n}_z being the unit vector along the z -axis. We will evaluate the fluxes in the interior and exterior regions with the integrations over $r \in [0, r_c]$ and $r \in [r_c, \infty)$, respectively. Substituting the Fourier expansions (3.19) and (3.22), after integration over ϕ we find

$$\begin{aligned} I^{(f)}(\xi) &= -\frac{c}{4} \int_0^\infty dr r \sum_{n=0}^\infty \sum_{s,s'} \sin(u_{n,s}\xi/r_c) \sin(u_{n,s'}\xi/r_c) \\ &\times \left[(1 + \delta_{0n}) E_{1,n}^{(P)}(u_{n,s}) H_{2,n}^{(P)}(u_{n,s'}) + (1 - \delta_{0n}) E_{2,n}^{(P)}(u_{n,s}) H_{1,n}^{(P)}(u_{n,s'}) \right], \end{aligned} \quad (4.2)$$

where the Fourier components are given by (3.20) and (3.23).

The energy flux through the plane $z = \text{const}$ during the time interval $z/v \leq t \leq t_0$ is given by $\mathcal{E}_{[z/v, t_0]}^{(f)} = \int_{z/v}^{t_0} dt I^{(f)}(\xi) = \int_0^{vt_0 - z} d\xi I^{(f)}(\xi)/v$. The difference of the corresponding fluxes for the planes $z = z_1$ and $z = z_2 > z_1$ is expressed as

$$\mathcal{E}^{(f)}(t_0, z_1, z_2) = \mathcal{E}_{[t_1, t_0]}^{(f)} - \mathcal{E}_{[t_2, t_0]}^{(f)} = \frac{1}{v} \int_{vt_0 - z_2}^{vt_0 - z_1} d\xi I^{(f)}(\xi), \quad (4.3)$$

where $t_j = z_j/v$, $j = 1, 2$. This difference characterizes the energy radiated by the charge during the time interval $t \in [t_1, t_2]$. In the limit $t_0 \rightarrow \infty$ we use the result

$$\lim_{t_0 \rightarrow \infty} \int_{vt_0 - z_2}^{vt_0 - z_1} d\xi \sin(u\xi/r_c) \sin(u'\xi/r_c) = \frac{t_2 - t_1}{2v} \delta_{u'u}. \quad (4.4)$$

By using (4.2), for the mean energy flux (averaged in the way described above) per unit time through the plane $z = \text{const}$, given by $I^{(f)} = \lim_{t_0 \rightarrow \infty} \mathcal{E}^{(f)}(t_0, z_1, z_2)/(t_2 - t_1)$, we get

$$I^{(f)} = -\frac{c}{8} \int_0^\infty dr r \sum_{n=0}^\infty \sum_s \left[(1 + \delta_{0n}) E_{1,n}^{(P)}(u) H_{2,n}^{(P)}(u) + (1 - \delta_{0n}) E_{2,n}^{(P)}(u) H_{1,n}^{(P)}(u) \right]_{u=u_{n,s}}. \quad (4.5)$$

We write the total energy flux in the form

$$I^{(f)} = \sum_{n=0}^{\infty} \sum_s \left(I_{i,n,s}^{(f)} + I_{e,n,s}^{(f)} \right),$$

where $I_{i,n,s}^{(f)}$ and $I_{e,n,s}^{(f)}$ are the energy fluxes on a given mode $u = u_{n,s}$ in the regions $r < r_c$ (interior) and $r > r_c$ (exterior). Those separate contributions are obtained from (4.5) by using the expressions for the Fourier components of the electric and magnetic fields given in the previous section. The corresponding radial integrals are reduced to [50]

$$\begin{aligned} \int_0^{r_c} dr r I_{n+p}^2(\gamma_0 u r / r_c) &= \frac{r_c^2}{2} [I_{n+p}^2(\gamma_0 u) - I_{n+2p}(\gamma_0 u) I_n(\gamma_0 u)], \\ \int_{r_c}^{\infty} dr r K_{n+p}^2(\gamma_1 u r / r_c) &= \frac{r_c^2}{2} [K_{n+2p}(\gamma_1 u) K_n(\gamma_1 u) - K_{n+p}^2(\gamma_1 u)]. \end{aligned} \quad (4.6)$$

For the energy flux in the region $r < r_c$ we find

$$\begin{aligned} I_{i,n,s}^{(f)} &= \delta_n \frac{q^2 v}{4r_c^2} \frac{Q_n^2(u)}{\varepsilon_0} \sum_{p,p'=\pm 1} (1 + pp' \beta^2 \varepsilon_0) \frac{K_{n+p'}(\gamma_1 u)}{W_{n+p'}^I} \\ &\quad \times \frac{K_{n+p}(\gamma_1 u)}{W_{n+p}^I} [I_{n+p}^2(\gamma_0 u) - I_{n+2p}(\gamma_0 u) I_n(\gamma_0 u)] |_{u=u_{n,s}}. \end{aligned} \quad (4.7)$$

Note that by using the first relation in (3.25) one has

$$\sum_{p'=\pm 1} (1 + pp' \beta^2 \varepsilon_0) \frac{K_{n+p'}(\gamma_1 u)}{W_{n+p'}^I} = 2p\varepsilon_0 \left[\beta^2 \frac{K_{n+1}(\gamma_1 u)}{W_{n+1}^I} - \frac{p - \beta_0^2}{(\varepsilon_0 - \varepsilon_1) \gamma_0 I_n(\gamma_0 u)} \right]. \quad (4.8)$$

By taking into account that $W_{n+p}^I < 0$, from (4.7) we see that the energy flux is always positive.

In a similar way, for the energy flux of SPs in the exterior region, $r > r_c$, one gets

$$\begin{aligned} I_{e,n,s}^{(f)} &= \delta_n \frac{q^2 v}{4r_c^2} \frac{Q_n^2(u)}{\varepsilon_1} \sum_{p,p'=\pm 1} (1 + pp' \beta^2 \varepsilon_1) \frac{I_{n+p'}(\gamma_0 u)}{W_{n+p'}^I} \\ &\quad \times \frac{I_{n+p}(\gamma_0 u)}{W_{n+p}^I} [K_{n+2p}(\gamma_1 u) K_n(\gamma_1 u) - K_{n+p}^2(\gamma_1 u)] |_{u=u_{n,s}}. \end{aligned} \quad (4.9)$$

From the second relation in (3.25) we have

$$\sum_{p'=\pm 1} (1 + pp' \beta^2 \varepsilon_1) \frac{I_{n+p'}(\gamma_0 u)}{W_{n+p'}^I} = 2p\varepsilon_1 \left[\beta^2 \frac{I_{n+1}(\gamma_0 u)}{W_{n+1}^I} + \frac{p - \beta^2 \varepsilon_1}{(\varepsilon_0 - \varepsilon_1) \gamma_1 K_n(\gamma_1 u)} \right]. \quad (4.10)$$

For the average total energy flux on a given mode $k_{n,s} = u_{n,s}/r_c$ we have

$$I_{t,n,s}^{(f)} = I_{i,n,s}^{(f)} + I_{e,n,s}^{(f)}. \quad (4.11)$$

By taking into account that for given values of β_0 and $\varepsilon_1/\varepsilon_0$ the roots do not depend on r_c and r_0 , we see that the dependence of the energy fluxes on those parameters appears in the form $I_n^2(\gamma_0 u r_0 / r_c) / r_c^2$. In particular, for a fixed ratio r_0/r_c the fluxes decay as $1/r_c^2$ with increasing radius of the cylinder. In the non-relativistic limit, to the leading order, the modes $u_{n,s}$ are roots of the equation (3.37) and

for given $\varepsilon_1/\varepsilon_0$ do not depend on the charge velocity. In the same order, one has $\gamma_j \approx 1$, $j = 0, 1$, and from (4.7) and (4.9) we conclude that the energy fluxes behave as $I_{j,n,s}^{(f)} \propto \beta$, $j = i, e$, for $\beta \ll 1$.

Let us consider the asymptotic behavior of the energy fluxes for large values $u = u_{n,s}$. As it has been discussed above, this asymptotic is realized in the range of dielectric permittivities where

$$\varepsilon_1/\varepsilon_0 \approx -\gamma_0^{-2}. \quad (4.12)$$

For the asymptotic of the function $\bar{\alpha}_n(u)$ at the points $u = u_{n,s}$ we get

$$\bar{\alpha}_n(u) \approx \frac{\varepsilon_1/\varepsilon_0 + \varepsilon_0/\varepsilon_1 + 1 + 2\beta_0^2 u/\gamma_0}{2\gamma_0 (1 - \varepsilon_1/\varepsilon_0) u^2}. \quad (4.13)$$

Note that in the numerator we have kept additional terms to include in the asymptotic analysis the region $\beta_0^2 u \lesssim 1$. By using the asymptotic expressions of the modified Bessel functions for large argument [49] it can be seen that, to the leading order,

$$I_{i,n,s}^{(f)} \approx \frac{4\delta_n q^2 v (1 - \varepsilon_0/\varepsilon_1)^{-2} u_{n,s}^3 \gamma_0 e^{-2(1-r_0/r_c)\gamma_0 u_{n,s}}}{r_0 r_c \varepsilon_0 (\varepsilon_1/\varepsilon_0 + \varepsilon_0/\varepsilon_1 + 1 + 2\beta_0^2 u_{n,s}/\gamma_0)^2}. \quad (4.14)$$

In a similar way, for the energy flux in the exterior medium one gets

$$I_{e,n,s}^{(f)} \approx -\frac{4\delta_n q^2 v (1 - \varepsilon_1/\varepsilon_0)^{-2} u_{n,s}^3 \gamma_0 e^{-2(1-r_0/r_c)\gamma_0 u_{n,s}}}{r_0 r_c \varepsilon_0 (\varepsilon_1/\varepsilon_0 + \varepsilon_0/\varepsilon_1 + 1 + 2\beta_0^2 u_{n,s}/\gamma_0)^2}. \quad (4.15)$$

For the total energy flux this gives

$$I_{t,n,s}^{(f)} \approx \frac{4\delta_n q^2 v}{r_0 r_c \varepsilon_0} \frac{u_{n,s}^3 \gamma_0 e^{-2(1-r_0/r_c)\gamma_0 u_{n,s}}}{(\varepsilon_1/\varepsilon_0 + \varepsilon_0/\varepsilon_1 + 1 + 2\beta_0^2 u_{n,s}/\gamma_0)^2} \frac{\varepsilon_1 + \varepsilon_0}{\varepsilon_1 - \varepsilon_0}. \quad (4.16)$$

The energy flux is positive/negative in the medium with positive/negative dielectric permittivity. From (4.12) it follows that $\varepsilon_1 + \varepsilon_0 < 0$ and the total energy flux is positive. The exponent in the asymptotic expressions (4.14) and (4.15) is written as $2(1 - r_0/r_c)\gamma_0 u_{n,s} = 4\pi(r_c - r_0)\gamma_0/\lambda_{n,s}$ and we see that the energy fluxes for a given radiation wavelength are exponentially suppressed if the distance of the charge trajectory from the cylinder surface is much larger than the wavelength. The suppression factor decreases with increasing velocity of the charge. We could expect the exponential suppression of energy fluxes for large values of $u_{n,s}$. The SP for a given frequency is generated by the corresponding spectral component of the charge proper field. For a charge moving with constant velocity and at distances from the trajectory larger than the wavelength the spectral component of the field is exponentially small. The exponential factor in the asymptotic expressions (4.14) and (4.15) is directly related to the corresponding suppression factor in the proper field of the charge. Note that in obtaining the asymptotics for large u we have used approximate expressions for the modified Bessel functions which are valid for $n \ll \gamma_j u$.

In order to see the features of the energy fluxes for large values of the azimuthal quantum number n we use the corresponding uniform asymptotic expansions of the modified Bessel functions [49]. Those expansions contain the exponential factor $e^{-n\eta(x/n)}$ for the function $K_n(x)$ and the factor $e^{n\eta(x/n)}$ for $I_n(x)$, where

$$\eta(x) = \sqrt{1+x^2} + \ln \frac{x}{1 + \sqrt{1+x^2}}. \quad (4.17)$$

For the related exponential factors in the expressions of the energy fluxes we get

$$I_{j,n,s}^{(f)} \propto e^{2n[\eta(\gamma_0 u r_0/n r_c) - \eta(\gamma_0 u/n)]}, \quad j = i, e, \quad (4.18)$$

with $u = u_{n,s}$. For $\gamma_j u \gg n$ the exponent in (4.18) is reduced to the one in (4.14) and (4.15). Note that $\eta'(x) = \sqrt{1+x^2}/x$ and the function $\eta(x)$ is monotonically increasing for $x > 0$. As a consequence, the exponent in (4.18) is negative. As it has been already discussed in Section 3, for large n two qualitatively different possibilities are realized. If for the corresponding frequencies the permittivity ε_1 is sufficiently close to $-\varepsilon_0$ (see (3.32)), we have $u_{n,s} \ll n$ and the arguments of the functions $\eta(x)$ in (4.18) are small. In this regime, to the leading order one gets $I_{j,n,s}^{(f)} \propto (r_0/r_c)^{2n}$. In the second case, ε_1 and $-\varepsilon_0$ are not too close and the modes $u_{n,s}$ are approximated by (3.33). The corresponding exponential factors in the expressions for the energy fluxes are obtained from (4.18) by the replacement $u/n \rightarrow 1/\sqrt{\beta_0^2 \varepsilon_1 / (\varepsilon_0 + \varepsilon_1) - 1}$.

In the special case of the axial motion the SPs are radiated only on the mode $n = 0$. For given β_0 and $\varepsilon_1/\varepsilon_0$ there is a single mode $u = u_0$ and it is the root of the equation (3.39). By using that equation, the expressions for the interior and exterior fluxes are simplified as

$$I_{i,0}^{(f)} = \frac{q^2 v}{2r_c^2 \varepsilon_0} \frac{\varepsilon_0^2}{\varepsilon_1^2} \frac{\left[\frac{I_1(\gamma_0 u)}{I_0(\gamma_0 u)} + \frac{1}{\gamma_0 u} \right]^2 - \frac{1}{\gamma_0^2 u^2} - 1}{(1 - \varepsilon_0/\varepsilon_1)^4 I_1^2(\gamma_0 u) \bar{\alpha}_0^2(u)}, \quad (4.19)$$

and

$$I_{e,0}^{(f)} = -\frac{q^2 v}{2r_c^2 \varepsilon_1} \frac{\gamma_0^2}{\gamma_1^2} \frac{\left[\frac{K_1(\gamma_1 u)}{K_0(\gamma_1 u)} - \frac{1}{\gamma_1 u} \right]^2 - \frac{1}{\gamma_1^2 u^2} - 1}{(1 - \varepsilon_0/\varepsilon_1)^4 I_1^2(\gamma_0 u) \bar{\alpha}_0^2(u)}, \quad (4.20)$$

with $u = u_0$. We can see that $I_{e,0}^{(f)} < 0 < I_{i,0}^{(f)}$. By taking into account that the root u_0 does not depend on r_c , we conclude that for fixed values of the other parameters the energy fluxes, as functions of the cylinder radius, behave like $1/r_c^2$.

We recall that for a given n the roots $u_{n,s}$ are determined by β_0 and $\varepsilon_1/\varepsilon_0$: $u_{n,s} = u_{n,s}(\beta_0, \varepsilon_1/\varepsilon_0)$. From (4.7) and (4.9) it is seen that the dimensionless combination $\varepsilon_0 r_c^2 I_{j,n,s}^{(f)} / (q^2 v)$, with $j=i,e,t$, is completely determined by the values β_0 , $\varepsilon_1/\varepsilon_0$, and r_0/r_c . That combination corresponds to the energy flux radiated by the charge from the part of trajectory of the length r_c , measured in units of $q^2/\varepsilon_0 r_c$. In Figure 6 we display the energy fluxes for radiated SPs in the exterior and interior regions as functions of $u_{n,s} = 2\pi r_c / \lambda_{n,s}$, with $\lambda_{n,s}$ being the wavelength. In the numerical evaluation we have taken $\beta_0 = 0.9$ and $r_0/r_c = 0.95$. The left and right panels correspond to $\varepsilon_0/\varepsilon_1 = -3$ and $\varepsilon_0/\varepsilon_1 = -1.5$, respectively. The plot markers circles, squares and diamonds correspond to the interior, $I_{i,n,s}^{(f)}$, exterior, $I_{e,n,s}^{(f)}$, and total, $I_{n,s}^{(f)}$, energy fluxes, respectively. The modes $u_{n,s}$ on the horizontal axis of the left panel correspond to the modes with $0 \leq n \leq 45$, whereas on the right panel $0 \leq n \leq 60$. In general, the roots $u_{n,s}$ are not monotonic functions of n , though that is the case for large n . For example, in the case $\varepsilon_0/\varepsilon_1 = -1.5$ one has $u_{0,s} \approx 2.61$, $u_{1,s} \approx 1.74$, and $u_{2,s} \approx 2.46$. As seen, the energy flux is directed along the charge motion in the interior region (with positive dielectric permittivity) and along the negative direction of z -axis in the exterior region (with negative dielectric permittivity). The total energy flux is dominated by the contribution of the interior region.

Figure 7 presents the dependence of the energy fluxes on $u_{n,s}$ for $\beta_0 = 0.75$, $r_0/r_c = 0.95$. The left panel is plotted for $\varepsilon_1/\varepsilon_0 = -1.5$ and for the right panel $\varepsilon_1/\varepsilon_0 = -1.1$. As it has been already mentioned above, the energy fluxes are exponentially suppressed for large values of $u_{n,s}$ corresponding to small wavelengths. The exponent of the suppression factor is expressed as $2(1 - r_0/r_c) \gamma_0 u_{n,s}$ and the characteristic value of $u_{n,s}$, given by $1/[2(1 - r_0/r_c) \gamma_0]$, is equal to ≈ 23 and ≈ 15 for the parameters corresponding to Figures 6 and 7. These numbers are in agreement of the numerical data in figures.

In Figure 8 we have presented the energy fluxes for SPs versus n , $0 \leq n \leq 80$, in the case when the dispersion of the dielectric function for the medium in the region $r > r_c$ is described by (3.34) and for the interior region we have taken $\varepsilon_0 = 1$. The fluxes are evaluated for $r_c \omega_p / c = 15$ and $r_0/r_c = 0.95$.

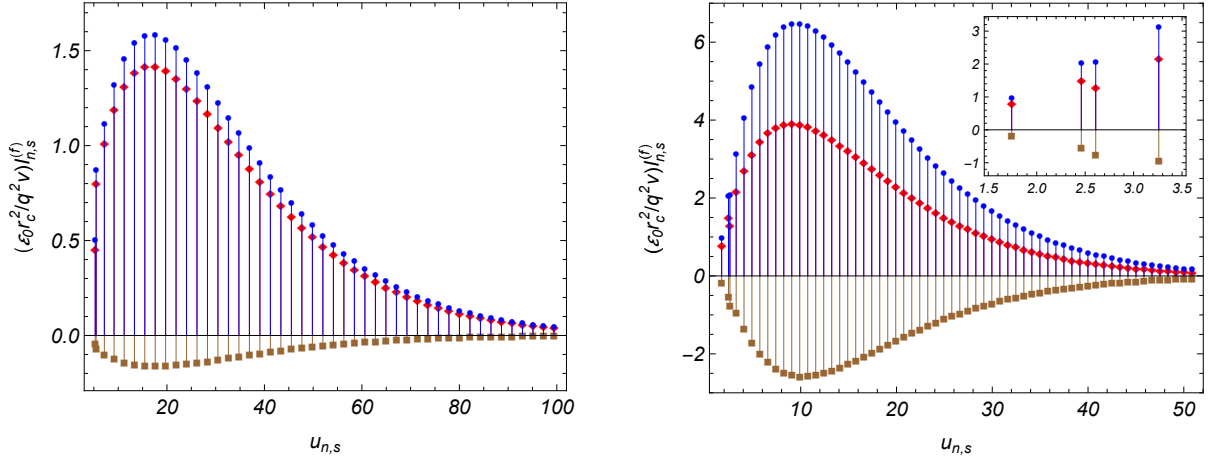


Figure 6: Energy fluxes of the radiated SPs inside (circles) and outside (squares) the cylinder versus $u_{n,s}$. The points marked by diamonds correspond to the total energy flux. The graphs are plotted for $\beta_0 = 0.9$, $r_0/r_c = 0.95$, and for two values of the ratio of dielectric permittivities: $\varepsilon_1/\varepsilon_0 = -3$ (left panel) and $\varepsilon_1/\varepsilon_0 = -1.5$ (right panel).

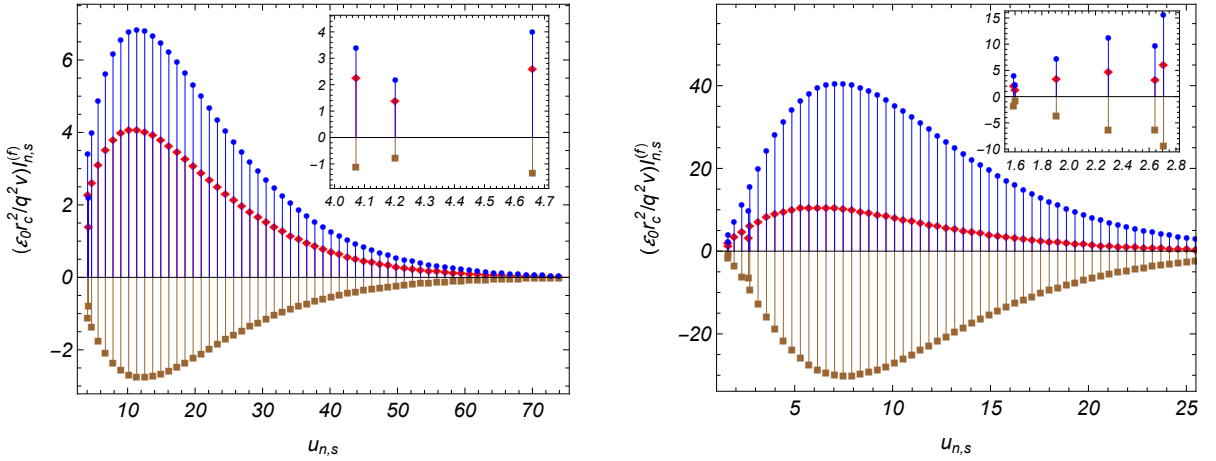


Figure 7: The same as in Figure 6 for $\beta_0 = 0.75$. The left and right panels correspond to $\varepsilon_1/\varepsilon_0 = -1.5$ and $\varepsilon_1/\varepsilon_0 = -1.1$, respectively.

The left and right panels are plotted for $v/c = 0.9$ and $v/c = 0.5$, respectively. For the example on the left panel the frequencies $\omega = \omega_n$ monotonically increase with increasing n and quickly converges to the limit $1/\sqrt{2}$ for large n . One has $\omega_n/\omega_p \approx 0.4611$ for $n = 0$ and $\omega_n/\omega_p \approx 0.7041$ for $n = 80$. We have similar behavior in the example of the right panel with $\omega_n/\omega_p \approx 0.6655$ for $n = 0$ and $\omega_n/\omega_p \approx 0.7043$ for $n = 80$. In both cases the function $\varepsilon_1(\omega)$ tends to -1 . As it has been explained above, for the model of dispersion at hand and for large n the eigenfrequencies of the radiated SPs are localized in the narrow range near the frequency $\omega_p/\sqrt{2}$. The data presented in Figure 8 show that the main part of the energy is radiated in that frequency range.

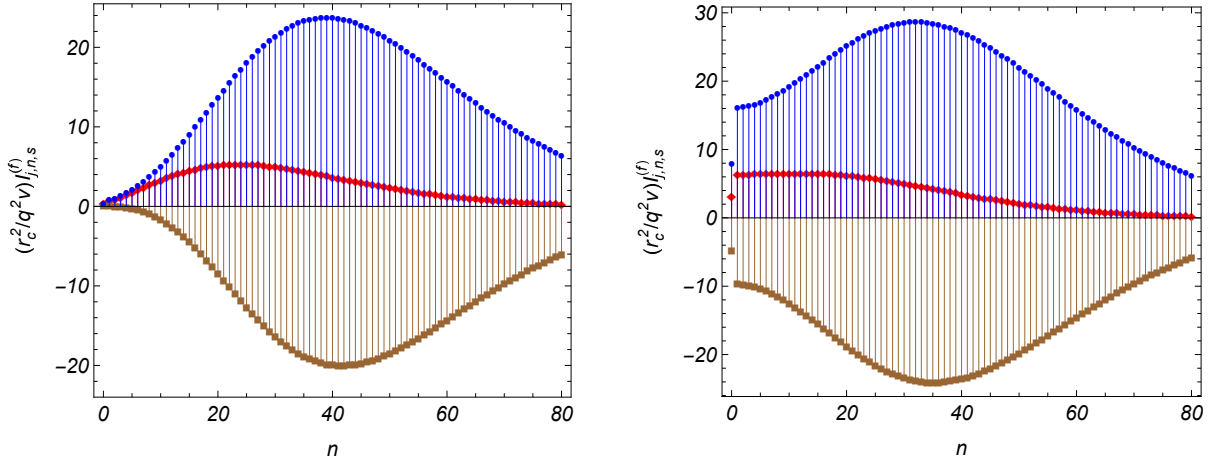


Figure 8: Energy fluxes for the SPs as functions of n for the dielectric function (3.34) and for $\varepsilon_0 = 1$. The points marked by circles, squares and diamonds correspond to the interior, exterior and total energy fluxes. For the parameters we have taken $r_0/r_c = 0.95$, $r_c\omega_p/c = 15$, and $\beta_0 = 0.9, 0.5$ for the left and right panels, respectively.

In Figures 9 and 10, the total energy flux is displayed as a function of the eigenfrequencies ω_n/ω_p of the surface polaritonic modes. As for the example in Figure 8, we have taken $\varepsilon_0 = 1$, $\varepsilon_1 = 1 - \omega_p^2/\omega^2$, and $0 \leq n \leq 80$. The numerical evaluation is done for $r_0/r_c = 0.95$, $r_c\omega_p/c = 10$. The left and right panels of Figure 9 correspond to $\beta_0 = 0.9$ and $\beta_0 = 0.75$. Correspondingly, the left and right panel of Figure 10 are plotted for $\beta_0 = 0.5$ and $\beta_0 = 0.25$. Note that, in order to show the dependence on the charge velocity, in Figures 9 and 10 we have presented the quantity $(r_c^2 q^2/c)I_{t,n,s}^{(f)}$ instead of $(r_c^2 q^2/v)I_{t,n,s}^{(f)}$ in Figure 8.

The numerical examples, we have discussed above for the properties of the roots and for the energy fluxes, are presented in terms of scale invariant combinations of the parameters. This allows to specify the corresponding results for different values of the cylinder radius. As already stated, for given β_0 and $\varepsilon_1/\varepsilon_0$ the SP eigenmodes with respect to $u = k_z r_c$ do not depend on the radius of the cylinder. The radiation wavelength, $\lambda_{n,s} = 2\pi r_c/u_{n,s}$, is controlled by the choice of the waveguide radius. The recent advances in nanofabrication allow to design cylindrical waveguides with radii in a sufficiently wide range, from millimeters to nanometers (see, e.g., Refs. [8, 51, 52]). One can control the wavelength of radiated SPs by an appropriate choice of the waveguide radius and negative-permittivity medium. Materials and artificially constructed subwavelength structures are available with plasma frequency in the visible, infrared and terahertz frequency ranges. The electron beam in TEMs provides an example of high quality source in relatively wide energy range from 50 keV to 500 keV. The same beam from TEMs can be used to drill nanometre-scale cylindrical holes in a medium.

Our main concern in the discussion above was the radiation for a single charge. Based on the results obtained, we can investigate the radiation from a bunch of N particles with velocities \mathbf{v}_m ,

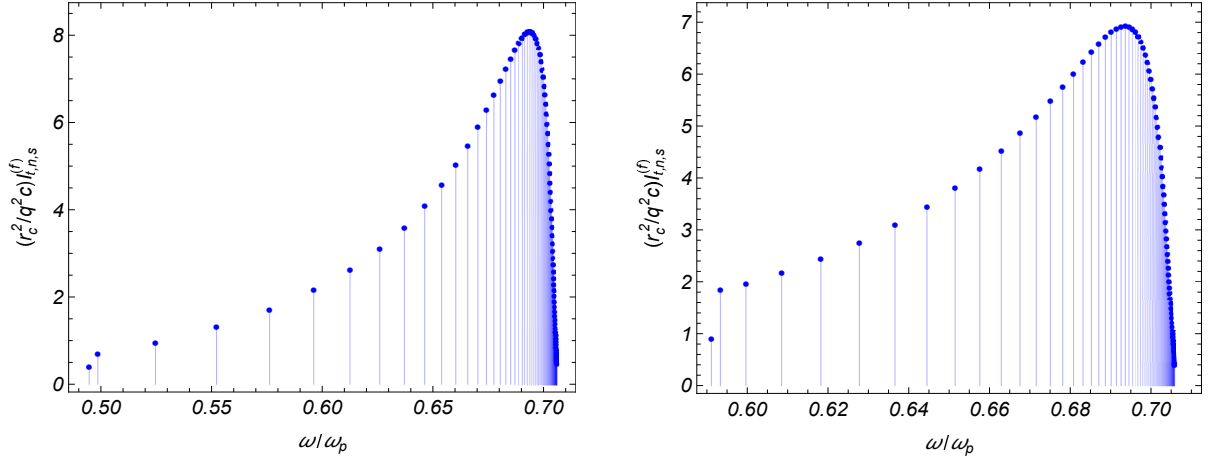


Figure 9: Total energy flux versus the eigenfrequencies of the surface polariton modes in the model with (3.34) and for $\varepsilon_0 = 1$ for the values of the parameters $r_0/r_c = 0.95$, $r_c \omega_p/c = 10$, and $\beta = 0.9, 0.75$ for the left and right panels.

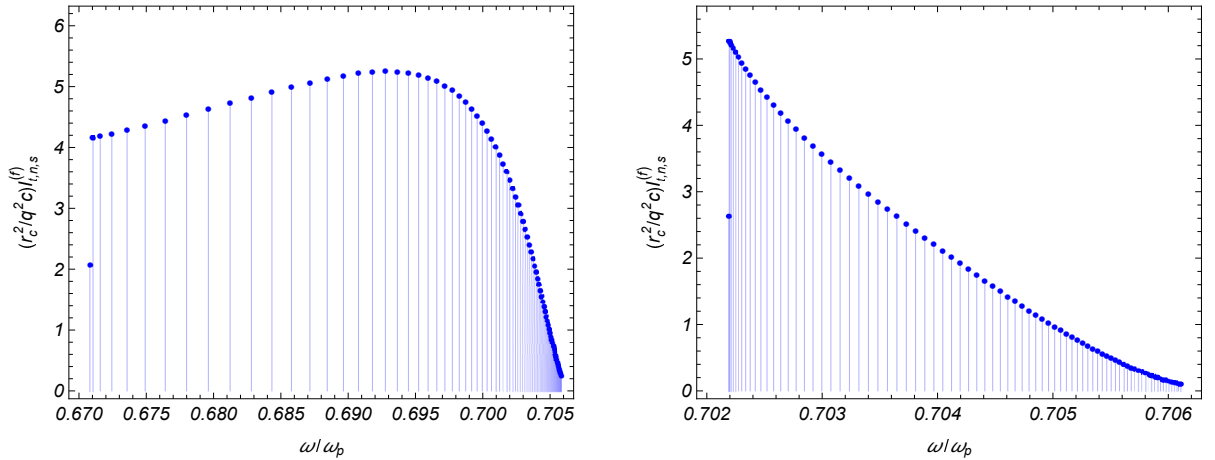


Figure 10: The same as in Figure 9 for $\beta = 0.5$ (left panel) and $\beta = 0.25$ (right panel).

$m = 1, 2, \dots, N$, parallel to the cylinder axis. For the current density one has

$$j_l(x) = \delta_{3l} q \sum_{m=1}^N \frac{v_m}{r_m} \delta(\mathbf{r} - \mathbf{r}_{0m}(t)), \quad (4.21)$$

where $\mathbf{r}_{0m}(t) = (r_m, \phi_m, z_m + v_m t)$ in cylindrical coordinates. Assuming that for all the particles $r_m < r_c$, the electromagnetic fields corresponding to the radiated SPs are obtained by summing the fields for separate charges. For example, the formula for the components of the vector potential reads

$$A_l^{(P)}(x) = \frac{2q}{cr_c} \sum_{m=1}^N v_m \sum_{n=0}^{\infty} \sum_s Q_{m,n}(u) \sum_{p=\pm 1} \frac{R_{m,n+p}(u, r/r_c)}{p^{l-1} u W_{m,n+p}^I} \\ \times \cos(u\xi_m/r_c) \sin[l\pi/2 - n(\phi - \phi_m)]|_{u=u_{m,n,s}}, \quad (4.22)$$

where $\xi_m = v_m t - z + z_m$ and the expressions for $R_{m,n}(u, r/r_c)$, $W_{m,n}^I$, $Q_{m,n}(u)$ are obtained from the corresponding expressions for the functions without the index m by the replacements $\gamma_j \rightarrow \gamma_{m,j} = \sqrt{1 - v_m^2 \varepsilon_j / c^2}$ and $r_0 \rightarrow r_m$. For monoenergetic bunches with transverse beam size smaller than the radiation wavelength (the specific condition will depend on the energy of the beam as well) we can approximate the general formula (4.22) taking $v_m = v$, $r_m = r_0$, $\phi_m = 0$. In this simple case the expressions for the radiation fields are obtained from the formulas given in Section 3 making the replacements $\cos(u\xi/r_c) \rightarrow \sum_m \cos(u\xi_m/r_c)$ and $\sin(u\xi/r_c) \rightarrow \sum_m \sin(u\xi_m/r_c)$. For the energy flux through the plane $z = \text{const}$ we get an expression which is obtained from (4.2) replacing the product of sin functions by $\sum_{m,m'} \sin(u_{n,s}\xi_m/r_c) \sin(u_{n,s'}\xi_{m'}/r_c)$. By using the same averaging procedure, we can see that the energy fluxes for SPs radiated by a bunch with longitudinal distribution function $f(z)$ are obtained from (4.7) and (4.9) adding the factor $N[1 + (N-1)|g(u/r_c)|^2]$ in the right-hand sides, where $g(w) = \int_{-\infty}^{+\infty} dz e^{-i w z} f(z)$ is the longitudinal bunch form factor. The second term in the square brackets describes the coherent effects in the radiation of SPs. Note that the longitudinal form factor depends on the frequency and on the monoenergetic bunch velocity in the form of the ratio ω/v . This property is a direct consequence of homogeneity of the problem under consideration along the z -direction. A similar longitudinal form factor appears also for other types of radiation processes, such as Cherenkov radiation, Smith-Purcell radiation, etc. (see, e.g., [53]-[57]). The coherence effects have been used to increase significantly the radiation intensity in different spectral ranges and also in beam diagnostics. For the radiation wavelengths of the order of transverse beam size or smaller the effect of the transverse form factor on the coherence properties becomes significant. In particular, the dependence on the energy of the beam is more pronounced.

In the discussion above we have considered an idealized problem where the dielectric permittivities of the media inside and outside the cylinder are taken to be real. A small imaginary part of the permittivity of the exterior medium was introduced in Section 2 in order to specify the contour of the integration over k_z near the poles, corresponding to the roots of the eigenmode equation for SPs. The approach we have described can be considered as a first step to the investigation of the surface polariton generation in more realistic setups with energy losses. The damping of SPs arising from the imaginary part of dielectric permittivity medium is one of the main limitations for practical applications in plasmonic devices. The energy dissipation, primarily in the form of Ohmic losses, limits the energy accumulated by SPs and may significantly reduce their propagation distances (for various decay channels of SPs energy dissipation see, e.g., [58]). In particular, that is the case for the commonly used plasmonic materials in the optical range such as silver and gold. Related to this, the development of various approaches and mechanisms aiming to reduce or compensate the energy losses remains among the main directions in plasmonics. They can be categorized into three main groups [58, 59, 60]. The first one is the choice of suitable material for negative-permittivity medium. The list of low loss plasmonic materials in mid infrared and terahertz spectral ranges include various

kinds of doped semiconductors, superconductors, transparent conducting oxides, different types of metamaterials, topological insulators and 2D Dirac materials like graphene (see, for example, Refs. [61]-[69] and references therein). An important advantage with these classes of plasmonic materials is the possibility to actively tune the plasma frequency. For example, that can be done by the choice of doping level in doped semiconductors and by electrostatic gating in graphene. The second direction to reduce the dissipative losses of surface plasmons corresponds to the engineering the shape and size of the structure along which the waves propagate. They include grating type structures with different geometries and metamaterials with controllable electromagnetic characteristics. And finally, the third direction of investigations uses gain media to compensate the energy losses of SPs.

Note that the expressions (2.4) and (2.5) are valid for general case of complex dielectric functions ε_0 and ε_1 , and they can be used for the evaluation of the electromagnetic fields in the problem at hand without specifying those functions. The scheme is similar to that we have described for the evaluation of the SP contributions: first we evaluate the vector potential by using Eq. (2.1) and then the scalar potential, electric and magnetic fields by standard formulas in classical electrodynamics. In the next section that procedure is described for the axial component of the electric field which determines the total energy losses of the charged particle.

5 Energy losses

In the discussion of the properties of the radiated SPs we have considered an idealized case where the imaginary part of the dielectric functions were ignored. We can investigate the total energy losses by a charged particle for general case of dielectric permittivities by using the expressions (2.3), (2.4) for the components of the Green tensor. Those expressions are also valid for dielectric functions having imaginary parts. Denoting by $\mathbf{E}(x)$ the electric field generated by the charge at the spacetime point $x = (t, \mathbf{r})$, the energy loss per unit length along the trajectory of the charge (the work of the field on the charge) is expressed as

$$\frac{dW}{dz} = qE_3(x)|_{\mathbf{r} \rightarrow \mathbf{r}_0(t)}. \quad (5.1)$$

By making use of the Fourier expansion for the axial component of the electric field,

$$E_3(x) = \sum_{n=-\infty}^{+\infty} \int_{-\infty}^{+\infty} dk_z E_{3,n}(k_z, r) e^{ik_z(z-vt)+in\phi}, \quad (5.2)$$

and the properties of the Fourier component $E_{3,n}(k_z, r)$, the formula is rewritten as

$$\frac{dW}{dz} = 2q \lim_{r \rightarrow r_0} \sum_{n=-\infty}^{+\infty} \operatorname{Re} \left[\int_0^\infty dk_z E_{3,n}(k_z, r) \right]. \quad (5.3)$$

The expression for $E_{3,n}(k_z, r)$ can be found based on the representations (2.4), by the scheme similar to that we have used in Section 3 for the contributions of SPs in the case of real dielectric functions ε_0 and ε_1 .

In this way, the energy losses are presented in the form

$$\frac{dW}{dz} = \frac{dW^{(0)}}{dz} - \frac{4q^2}{\pi r_c^2} \operatorname{Im} \left\{ \sum_{n=0}^{\infty} \delta_n \int_0^\infty du \frac{u\gamma_0^2}{\varepsilon_0 W_n^I} \left[W_n^K + \frac{K_n(u\gamma_1)}{2\gamma_0 u \alpha_n(u)} \sum_{p=\pm 1} \frac{K_{n+p}(u\gamma_1)}{W_{n+p}^I} \right] I_n^2(u\gamma_0 r_0 / r_c) \right\}, \quad (5.4)$$

where

$$\frac{dW^{(0)}}{dz} = \frac{2q^2}{\pi} \lim_{r \rightarrow r_0} \operatorname{Im} \left[\sum_{n=-\infty}^{\infty} \int_0^\infty dk_z \frac{k_z}{\varepsilon_0} \gamma_0^2 I_n(\gamma_0 k_z r_<) K_n(\gamma_0 k_z r_>) \right], \quad (5.5)$$

with $r_> = \max(r_0, r)$ and $r_< = \min(r_0, r)$. In the second term of (5.4) we have passed to the integration over u in accordance with (2.11) and the notation

$$W_n^K = \gamma_0 K_n(\gamma_1 u) K_{n+1}(\gamma_0 u) - \gamma_1 K_n(\gamma_0 u) K_{n+1}(\gamma_1 u), \quad (5.6)$$

is introduced. Other notations are the same as those used in the consideration above. However, now ε_0 and ε_1 , in general, are complex functions and, hence, the same is the case for γ_0 and γ_1 , defined in (3.4). The contribution (5.5) does not depend on the cylinder radius r_c and it corresponds to the energy losses in a homogeneous medium with dielectric permittivity ε_0 (bulk losses). These energy losses have been extensively investigated in the literature both theoretically and experimentally. Here we note that most of the previous studies consider the spectral density of the energy loss probability per unit length, $dP(\omega)/dz$, with the relation $dW/dz = \int_0^\infty d\omega \omega dP(\omega)/dz$. The series over n in (5.5) is summed by using the formula from [50] and we get

$$\frac{dW^{(0)}}{dz} = \frac{2q^2}{\pi} \lim_{r \rightarrow r_0} \text{Im} \left[\int_0^\infty dk_z \frac{k_z}{\varepsilon_0} \gamma_0^2 K_0(k_z |r - r_0| \sqrt{1 - \beta_0^2}) \right]. \quad (5.7)$$

For a transparent medium (ε_0 is real) and under the condition $\beta_0^2 < 1$, the integrand is real and $dW^{(0)}/dz = 0$. For transparent medium and under the Cherenkov condition $\beta_0^2 > 1$ the imaginary part of the Macdonald function in (5.7) is expressed in terms of the Bessel function as $\pi J_0(k_z |r - r_0| \sqrt{\beta_0^2 - 1})/2$. In this case the limit $r \rightarrow r_0$ can be taken directly in the integrand and from (5.7) we get the standard expression for the radiation intensity of the Cherenkov radiation in a homogeneous medium.

The second term on the right-hand side of (5.4) is induced by the difference of the dielectric permittivity in the region $r > r_c$ from ε_0 . By using the definitions for W_n^I , W_n^K , and $\alpha_n(u)$, the corresponding expression is written in more explicit form

$$\begin{aligned} \frac{dW}{dz} = & \frac{dW^{(0)}}{dz} - \frac{4q^2}{\pi r_c^2} \text{Im} \left\{ \sum_{n=0}^{\infty} \delta_n \int_0^\infty du \frac{u}{\varepsilon_0} \gamma_0^2 I_n^2(u \gamma_0 r_0 / r_c) \frac{K_n(\gamma_0 u)}{I_n(\gamma_0 u)} \right. \\ & \times \left. \frac{\left[\gamma_1 \frac{I_n'(\gamma_0 u)}{I_n(\gamma_0 u)} - \gamma_0 \frac{K_n'(\gamma_1 u)}{K_n(\gamma_1 u)} \right] \left[\varepsilon_0 \gamma_1 \frac{K_n'(\gamma_0 u)}{K_n(\gamma_0 u)} - \varepsilon_1 \gamma_0 \frac{K_n'(\gamma_1 u)}{K_n(\gamma_1 u)} \right] - \left(\frac{n\beta \varepsilon_0 - \varepsilon_1}{u \gamma_0 \gamma_1} \right)^2}{\left[\gamma_1 \frac{I_n'(\gamma_0 u)}{I_n(\gamma_0 u)} - \gamma_0 \frac{K_n'(\gamma_1 u)}{K_n(\gamma_1 u)} \right] \left[\varepsilon_0 \gamma_1 \frac{I_n'(\gamma_0 u)}{I_n(\gamma_0 u)} - \varepsilon_1 \gamma_0 \frac{K_n'(\gamma_1 u)}{K_n(\gamma_1 u)} \right] - \left(\frac{n\beta \varepsilon_0 - \varepsilon_1}{u \gamma_0 \gamma_1} \right)^2} \right\}. \quad (5.8) \end{aligned}$$

This expression coincides with that obtained from the energy loss probability found in [18]. Note that the zeros of the denominator determine the SP eigenmodes (compare with (3.13)). In the special case of the axial motion with $r_0 = 0$ the only nonzero contribution comes from the mode $n = 0$ and one gets

$$\frac{dW}{dz} = \frac{dW^{(0)}}{dz} + \frac{2q^2}{\pi r_c^2} \text{Im} \left[\int_0^\infty du \frac{u}{\varepsilon_0} \gamma_0^2 \frac{\varepsilon_0 \gamma_1 K_0(\gamma_1 u) K_1(\gamma_0 u) - \varepsilon_1 \gamma_0 K_1(\gamma_1 u) K_0(\gamma_0 u)}{\varepsilon_0 \gamma_1 K_0(\gamma_1 u) I_1(\gamma_0 u) + \varepsilon_1 \gamma_0 K_1(\gamma_1 u) I_0(\gamma_0 u)} \right]. \quad (5.9)$$

This result was obtained in [12, 14].

Another special case corresponds to the non-relativistic limit, $\beta \ll 1$. Assuming that $\beta^2 |\varepsilon_j| \ll 1$, $j = 0, 1$, to the leading order we can put $\gamma_j = 1$. In the same order, one gets $W_n^I \approx -1/u$, $W_n^K \approx 0$, and the function $\alpha_n(u)$ is approximated by (3.35). From (5.8), for the leading order contribution to the energy losses we find

$$\frac{dW}{dz} \approx \frac{dW^{(0)}}{dz} - \frac{4q^2}{\pi r_c^2} \sum_{n=0}^{\infty} \delta_n \text{Im} \left[\int_0^\infty du \frac{u}{\varepsilon_0} \frac{u K_n(u) K_n'(u) I_n^2(ur_0/r_c)}{\frac{\varepsilon_0}{\varepsilon_0 - \varepsilon_1} + u I_n(u) K_n'(u)} \right]. \quad (5.10)$$

The corresponding result for the energy loss probability has been widely discussed in the literature (see [9, 15, 16, 19, 21, 24, 28]).

For the numerical example of the energy losses we have considered the case where $\varepsilon_0 = 1$ and the dielectric function for the medium in the region $r > r_c$ is described by (3.34). In this special case one has $dW^{(0)}/dz = 0$. Let us introduce the spectral density of the energy loss per unit time, $dE_{(1)}(\omega)/d\omega$, in accordance with

$$\frac{dW}{dz} = -\frac{1}{v} \int_0^\infty d\omega \frac{dE_{(1)}}{d\omega}. \quad (5.11)$$

By using (5.4) we get

$$\frac{dE_{(1)}}{d\omega} = \frac{4q^2}{\pi r_c \gamma^2} \sum_{n=0}^{\infty} \text{Im} \left[u \frac{W_n^K}{W_n^I} + \frac{\gamma K_n(u\gamma_1)}{2\alpha_n(u)} \sum_{p=\pm 1} \frac{K_{n+p}(u\gamma_1)}{W_n^I W_{n+p}^I} \right] I_n^2 \left(\frac{ur_0}{\gamma r_c} \right), \quad (5.12)$$

where $\gamma = 1/\sqrt{1-\beta^2}$ is the relativistic factor and $u = r_c\omega/v$. Now, in the definitions of the functions W_n^I , W_n^K , and $\alpha_n(u)$ one has $\gamma_0 = 1/\gamma$. In Figure 11 the spectral density of the energy loss $dE_{(1)}(\omega)/d\omega$ is presented in units of q^2/r_c versus the ratio ω/ω_p . The graphs are plotted for $\eta/\omega_p = 10^{-2}$, $r_0/r_c = 0.95$, $\beta = 0.75$, and $r_c\omega_p/c = 10$. We have also displayed the separate contributions of the modes with different n , $dE_{(1)n}(\omega)/d\omega$, $0 \leq n \leq 25$, defined as $dE_{(1)}(\omega)/d\omega = \sum_{n=0}^{\infty} dE_{(1)n}(\omega)/d\omega$. For $n \geq 1$ the frequency corresponding to the maximum of $dE_{(1)n}(\omega)/d\omega$ increases with increasing n and the maximal value of that quantity decreases with increasing n . The curve with the minimal value for ω/ω_p at the peak correspond to the mode $n = 0$.

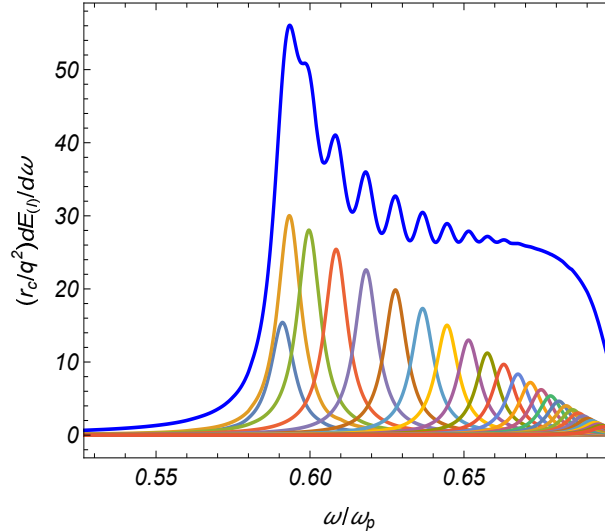


Figure 11: The spectral density of the energy loss per unit time as a function of frequency. The graphs are plotted for $\varepsilon_0 = 1$ and for the dispersion of the function $\varepsilon_1(\omega)$ described by (3.34) The values of the parameters are given in the text. The contributions of the modes with fixed n , $0 \leq n \leq 25$, are plotted as well.

6 Conclusion

We have investigated the radiation emitted by a charge uniformly moving inside a dielectric cylinder, parallel to its axis, assuming that the cylinder is loaded in a homogeneous medium. For evaluation

of the electromagnetic fields generated inside and outside the cylinder the Green tensor from [40] has been used. The corresponding expressions allow to study both the cases of the medium with negative dielectric permittivity in the spectral range under consideration inside and outside the cylinder. We have specified the investigation for the second case that will include the possibility of the charge motion in the vacuum. The required components of the Green tensor Fourier image are expressed as (2.4) and (2.5). Neglecting the imaginary part of dielectric permittivity, the Fourier components have poles corresponding to SPs. The respective contributions to the Green tensor are separated and they have been used in evaluating the field potentials and strengths inside and outside the cylinder. In general, both the transversal and longitudinal components of the electric and magnetic fields for excited SPs differ from zero. The fields exponentially decay in the exterior medium and they are mainly confined in the region of the thickness of the order $\lambda_{\text{sp}}/(2\pi\gamma_1)$ near the cylinder surface. The localization radius decreases with increasing velocity of the charge and it can be essentially smaller compared with the radiation wavelength λ_{sp} . The fields are expressed in terms of the eigenvalues for the projection of the wave vector along the cylinder axis and we have discussed their distribution as functions of the parameters and in the asymptotic regions. In particular, in the non-relativistic limit the SP modes are present in the region $-1 \leq \varepsilon_1/\varepsilon_0 < 0$ for the ratio of the dielectric functions. The relativistic effects may essentially enlarge the region for $\varepsilon_1/\varepsilon_0$ allowing the existence of the SP modes. We have specified the general consideration for the case of Drude dispersion in the exterior medium. The impact parameter r_0 enters in the expressions for the fields through the function $I_n(\gamma_0 u r_0 / r_c)$ in the definition (3.9) and, for a given frequency, the absolute values for the components of the fields monotonically increase with increasing r_0 . The general formulas are essentially simplified in the special case of axial motion when the only nonzero contribution to the radiation fields come from the mode with $n = 0$. In this special case the magnetic field is transversal and the electric and magnetic fields are orthogonal.

Having the electric and magnetic fields for SPs, in Section 4 we have evaluated the corresponding mean energy fluxes in the exterior and interior regions, given by (4.7) and (4.9). The exterior energy flux, corresponding to the negative-permittivity medium, is negative (flux along the direction opposite to the charge motion), whereas the flux inside the cylinder (positive-permittivity medium) is positive (directed along the direction of the charge motion). The total flux is dominated by the interior contribution and it is positive. In the non-relativistic limit the energy fluxes are proportional to the charge velocity. The relativistic effects may essentially increase the radiated energy. Other important features of relativism include the narrowing the confinement region of the SP fields near the cylinder surface in the exterior region, enlarging the frequency range for radiated SPs, and the decrease of the cutoff factor for radiation at small wavelengths compared with the cylinder radius. The energy fluxes at those wavelengths are approximated by (4.14) and (4.15). Relatively simple expressions for interior and exterior energy fluxes, (4.19) and (4.20), are obtained in the special case of the axial motion. The features clarified by asymptotic analysis of exact formulas are confirmed by numerical data. We have presented the latter in terms of dimensionless combinations of the parameters that allows to specify the results for different values of the waveguide radius and for different spectral ranges. Given the radiation fields generated by a single charge, the generalization is straightforward for a bunch of particles moving parallel to the axis of the cylinder. For example, the corresponding vector potential is expressed as (4.22). In the special case of a monoenergetic bunch with transverse size smaller than the radiation wavelength, the collective effects in the energy fluxes on a given frequency appear through the bunch longitudinal form factor.

By using the expressions for the components of the Green tensor, we have also considered the total energy losses for general case of dielectric functions of the exterior and interior media with imaginary parts. The general formula is given by (5.4) or, equivalently, by (5.8). The latter coincides with the result obtained from the energy loss probability previously considered in the literature and includes various special cases widely discussed before. Similar to the case of the SP energy fluxes, the numerical

analysis is provided in scale invariant form that allows to specify the result for special cases of the parameters (e.g., cylinder radius and plasma frequency for the negative-permittivity medium).

In our consideration the exterior medium occupies the region $r_c < r < \infty$. Based on the features described above, we expect that the obtained expressions of the SP energy fluxes for a given wavelength will approximate the corresponding results for the medium with finite extension, $r_c < r < r_{\text{ext}}$, if the thickness of the cylindrical layer $r_{\text{ext}} - r_c$ is larger than the confinement radius for the SPs on that wavelength. Note that the Green tensor in the problem with finite exterior layer can be found based on the recurrence procedure developed in [40] for general number of coaxial cylindrical layers. Another application of the results presented in this paper could be the investigation of the transversal forces acting on the charge in the case of paraxial motion. Those forces are of interest in studies of beam stabilities in particle accelerators. And finally, the problem we have considered is exactly solvable within the framework of classical electrodynamics and the corresponding results may serve as a tool to verify the accuracy of various approximate methods and simulations used for the investigation of surface polaritons in more complicated geometries of interfaces.

Acknowledgement

A.A.S. was supported by the Science Committee of RA, in the frames of the research project No. 21AG-1C047. L.Sh.G. and H.F.K. were supported by the Science Committee of RA, in the frames of the research project No. 21AG-1C069.

References

- [1] K. Welford, Surface plasmon-polaritons and their uses, *Optical and Quantum Electronics* **23**, 1 (1991).
- [2] V.M. Agranovich and D.L. Mills (Editors), *Surface Polaritons: Electromagnetic Waves at Surfaces and Interfaces* (North-Holland Pub. Co., Amsterdam, 1982).
- [3] S.A. Maier, *Plasmonics: Fundamentals and Applications* (Springer, 2007).
- [4] S. Enoch and N. Bonod (Editors), *Plasmonics: From Basics to Advanced Topics* (Springer, 2012).
- [5] M.I. Stockman *et al.*, Roadmap on plasmonics, *J. Optics* **20**, 043001 (2018).
- [6] R. Marqués, F. Martín, and M. Sorolla, *Metamaterials with Negative Parameters: Theory, Design, and Microwave Applications* (John Wiley & Sons, Hoboken, NJ, 2008).
- [7] Zh. Han and S.I. Bozhevolnyi, Radiation guiding with surface plasmon polaritons, *Rep. Prog. Phys.* **76**, 016402 (2013).
- [8] F.J. García de Abajo, Optical excitations in electron microscopy, *Rev. Mod. Phys.* **82**, 209 (2010).
- [9] A. Rivacoba, N. Zabala, and J. Aizpurua, Image potential in scanning transmission electron microscopy, *Prog. Surf. Sci.* **65**, 1 (2000).
- [10] E.J.R. Vesseur, J. Aizpurua, T. Coenen, A. Reyes-Coronado, P.E. Batson, and A. Polman, Plasmonic excitation and manipulation with an electron beam, *MRS Bulletin* **37**, 752 (2012).
- [11] L.S. Bogdankevich and B.M. Bolotovskii, Motion of a charge parallel to the axis of a cylindrical channel in a dielectric, *Sov. Phys. JETP* **5**, 1157 (1957).

- [12] B.M. Bolotovskii, Theory of Cherenkov radiation (III), *Sov. Phys. Uspekhi* **4**, 781 (1962).
- [13] Y.T. Chu et. al., Contribution of the surface plasmon to energy losses by electrons in a cylindrical channel, *Particle Accelerators* **16**, 13 (1984).
- [14] D. De Zutter and D. De Vleeschauwer, Radiation from and force acting on a point charge moving through a cylindrical hole in a conducting medium, *J. Appl. Phys.* **59**, 4146 (1986).
- [15] N. Zabala, A. Rivacoba, and P.M. Echenique, Energy loss of electrons travelling through cylindrical holes, *Surf. Sci.* **209**, 465 (1989).
- [16] C.A. Walsh, Analysis of electron energy-loss spectra from electron-beam-damaged amorphous AlF_3 , *Philos. Mag. A* **59**, 227 (1989).
- [17] M. Schmeits, Surface-plasmon coupling in cylindrical pores, *Phys. Rev. B* **39**, 7567 (1989).
- [18] C.A. Walsh, An analytical expression for the energy loss of fast electrons traveling parallel to the axis of a cylindrical interface, *Philos. Mag. B* **63**, 1063 (1991).
- [19] A. Rivacoba, P. Ape, and N. Zabala, Energy loss probability of STEM electrons in cylindrical surfaces. *Nucl. Inst. and Meth. B* **96**, 465 (1995).
- [20] J.M. Pitarke and A. Rivacoba, Electron energy loss for isolated cylinders, *Surf. Sci.* **377-379**, 294 (1997).
- [21] N.R. Arista and M.A. Fuentes, Interaction of charged particles with surface plasmons in cylindrical channels in solids, *Phys. Rev. B* **63**, 165401 (2001).
- [22] N. Zabala, E. Ogando, A. Rivacoba, and F. J. García de Abajo, Inelastic scattering of fast electrons in nanowires: A dielectric formalism approach, *Phys. Rev. B* **64**, 205410 (2001).
- [23] Y.-N. Wang and Z. L. Mišković, Energy loss of charged particles moving in cylindrical tubules, *Phys. Rev. A* **66**, 042904 (2002).
- [24] J.L. Gervasoni and N.R. Arista, Plasmon excitation in cylindrical wires by external charged particles. *Phys. Rev. B* **68**, 235302 (2003).
- [25] A.A. Aligia, J.L. Gervasoni, and N.R. Arista, Stopping force on point charges in cylindrical wires. *Phys. Rev. B* **70**, 235331 (2004).
- [26] Y.H. Tu, C.M. Kwei, and C.J. Tung, Inelastic interactions of electrons with cylindrical interfaces, *Surf. Sci.* **600**, 820 (2006).
- [27] S. Segui, J.L. Gervasoni, and N.R. Arista, Plasmon excitation in nanotubes. Comparison with capillaries and wires, *Radiat. Phys. Chem.* **76**, 582 (2007).
- [28] J.M. Pitarke, V.M. Silkin, E.V. Chulkov, and P.M. Echenique, Theory of surface plasmons and surface-plasmon polaritons. *Rep. Prog. Phys.* **70**, 1 (2007).
- [29] J. Aizpurua and A. Rivacoba, Nonlocal effects in the plasmons of nanowires and nanocavities excited by fast electron beams, *Phys. Rev. B* **78**, 035404 (2008).
- [30] J.K. Hyun, M.P. Levendorf, M. Blood-Forsythe, J. Park, and D.A. Muller, Relativistic electron energy loss spectroscopy of solid and core-shell nanowires, *Phys. Rev. B* **81**, 165403 (2010).

- [31] S.V. Yalunin, B. Schröder, and C. Ropers, Theory of electron energy loss near plasmonic wires, nanorods, and cones, *Phys. Rev. B* **93**, 115408 (2016).
- [32] N.R. Arista, J.L. Gervasoni, S. Segui, I. Villó-Pérez, and R.O. Barrachina, Plasmon excitation by charged particles in solids, surfaces, and nanostructures: Following the trail of R.H. Ritchie, *Advances in Quantum Chemistry* **80**, 271 (2019).
- [33] A.S. Kotanjyan, A.R. Mkrtchyan, A.A. Saharian, and V.Kh. Kotanjyan, Generation of surface polaritons in dielectric cylindrical waveguides, *Phys. Rev. Spec. Top. Accel. Beams* **22**, 040701 (2019).
- [34] A.A. Saharian, L.Sh. Grigoryan, A.Kh. Grigorian, H.F. Khachatryan, and A.S. Kotanjyan, Cherenkov radiation and emission of surface polaritons from charges moving paraxially outside a dielectric cylindrical waveguide, *Phys. Rev. A* **102**, 063517 (2020).
- [35] T. Stöckli, Z.L. Wang, J.-M. Bonard, P. Stadelmann, and A. Châtelain, Plasmon excitations in carbon nanotubes, *Philos. Mag. B* **79** (10), 1531 (1999).
- [36] T. Stöckli, J.-M. Bonard, A. Châtelain, Z.L. Wang, and P. Stadelmann, Collective oscillations in a single-wall carbon nanotube excited by fast electrons, *Phys. Rev. B* **64**, 115424 (2001).
- [37] D. Taverna, M. Kociak, V. Charbois, and L. Henrard, Electron energy-loss spectrum of an electron passing near a locally anisotropic nanotube. *Phys. Rev. B* **66**, 235419 (2002).
- [38] Y.-N. Wang and Z.L. Mišković, Interaction of fast ions with carbon nanotubes: self energy and stopping power. *Phys. Rev. A* **69**, 022901 (2004).
- [39] D.J. Mowbray, S. Segui, J. Gervasoni, Z.L. Mišković, and N.R. Arista, Plasmon excitations on a single-wall carbon nanotube by external charges: Two-dimensional two-fluid hydrodynamic model, *Phys. Rev. B* **82**, 035405 (2010).
- [40] L.Sh. Grigoryan, A.S. Kotanjyan, and A.A. Saharian, Green function of an electromagnetic field in cylindrically symmetric inhomogeneous medium, *Izv. Nats. Akad. Nauk Arm., Fiz.* **30**, 239 (1995) (Engl. Transl.: *J. Contemp. Phys.*).
- [41] A.A. Saharian and A.S. Kotanjyan, Synchrotron radiation from a charge moving along a helical orbit inside a dielectric cylinder, *J. Phys. A* **38**, 4275 (2005).
- [42] A.A. Saharian and A.S. Kotanjyan, Synchrotron radiation from a charge moving along a helix around a dielectric cylinder, *J. Phys. A* **42**, 135402 (2009).
- [43] A.A. Saharian and A.S. Kotanjyan, Synchrotron radiation inside a dielectric cylinder, *Int. J. Mod. Phys. B* **26**, 1250033 (2012).
- [44] A.S. Kotanjyan, A.R. Mkrtchyan, A.A. Saharian, and V.Kh. Kotanjyan, Radiation of surface waves from a charge rotating around a dielectric cylinder, *J. Instrum.* **13**, C01016 (2018).
- [45] A.A. Saharian, A.S. Kotanjyan, and V.Kh. Kotanjyan, Synchrotron radiation from a charge on eigenmodes of a dielectric cylinder, *J. Contemp. Phys.* **54**, 111 (2019).
- [46] J.C. Ashley and L.C. Emerson, Dispersion relations for nonradiative surface plasmons on cylinders, *Surf. Sci.* **41**, 615 (1974).
- [47] H. Khosravi, D. R. Tilley, and R. Loudon, Surface polaritons in cylindrical optical fibers, *J. Opt. Soc. Am. A* **8**, 112 (1991).

- [48] J.D. Jackson, *Classical Electrodynamics* (Wiley, New York, 1999).
- [49] *Handbook of Mathematical Functions*, edited by M. Abramowitz and I.A. Stegun (Dover, New York, 1972).
- [50] A.P. Prudnikov, Yu.A. Brychkov, and O.I. Marichev, *Integrals and Series* (Gordon and Breach, New York, 1986), Vol. 2.
- [51] S. Atakaramians, V.S. Afshar, T.M. Monro, and D. Abbott, Terahertz dielectric waveguides, *Adv. Opt. Photonics* **5**, 169 (2013).
- [52] Md. S. Islam, C.M.B. Cordeiro, M.A.R. Franco, J. Sultana, A.L.S. Cruz, and D. Abbott, Terahertz optical fibers, *Optics Express* **28**, 16089 (2020).
- [53] Y. Shibata, et. al., Coherent Smith-Purcell radiation in the millimeter-wave region from a short-bunch beam of relativistic electrons, *Phys. Rev. E* **57**, 1061 (1998).
- [54] A.A. Saharian, A.R. Mkrtchyan, L.A. Gevorgian, L.Sh. Grigoryan, and B.V. Khachatryan, Radiation from an electron bunch flying over a surface wave, *Nucl. Instrum. Methods Phys. Res., Sect. B* **173**, 211 (2001).
- [55] A.P. Potylitsyn, M.I. Ryazanov, M.N. Strikhanov, and A.A. Tishchenko, *Diffraction Radiation from Relativistic Particles* (Springer, Berlin, 2010).
- [56] S.Yu. Gogolev and A.P. Potylitsyn, Azimuthal asymmetry of coherent Cherenkov radiation from a tilted bunch, *Phys. Lett. A* **383**, 888 (2019).
- [57] Y. Tadenuma et.al., Generation of coherent THz Cherenkov radiation by electron bunch tilt control, *Phys. Rev. Spec. Top. Accel. Beams* **25**, 110102 (2022).
- [58] S.V. Boriskina, T.A. Cooper, L. Zeng, G. Ni, J.K. Tong, Y. Tsurimaki, Y. Huang, L. Meroueh, G. Mahan, and G. Chen, Losses in plasmonics: from mitigating energy dissipation to embracing loss-enabled functionalities, *Adv. Opt. Photon.* **9(4)**, 775 (2017).
- [59] A. Boltasseva and H.A. Atwater. Low-loss plasmonic metamaterials, *Science*, **331**(6015), 290 (2011).
- [60] J.B. Khurgin and A. Boltasseva, Reflecting upon the losses in plasmonics and metamaterials, *MRS Bulletin*, **37**(08), 768 (2012).
- [61] W.-S. Chang, B.A. Willingham, L.S. Slaughter, B.P. Khanal, L. Vigderman, E.R. Zubarev, and S. Link, Low absorption losses of strongly coupled surface plasmons in nanoparticle assemblies. *PNAS* **108**, 19879 (2011).
- [62] T. Low and P. Avouris, Graphene plasmonics for terahertz to midinfrared applications, *ACS Nano* **8**(2),1086 (2014).
- [63] T.M. Wijesinghe, M. Premaratne, and G.P. Agrawal, Low-loss dielectric-loaded graphene surface plasmon polariton waveguide based biochemical sensor, *J. Appl. Phys.* **117**, 213105 (2015).
- [64] Y. Hajati, Z. Zambouri, and M. Sabaeian, Low-loss and high-performance mid-infrared plasmon-phonon in graphene-hexagonal boron nitride waveguide, *J. Opt. Soc. Am. B.* **35**, 446 (2018).
- [65] Y. Li, I. Liberal, and N. Engheta, Structural dispersion-based reduction of loss in epsilon-near-zero and surface plasmon polariton waves, *Sci. Adv.* **5**, eaav3764 (2019).

- [66] K. Zheng, Y. Yuan, L. Zhao, Y. Chen, F. Zhang, J. Song, and J. Qu, Ultra-compact, low-loss terahertz waveguide based on graphene plasmonic technology, *2D Mater.* **7**, 015016 (2020).
- [67] D. Teng, Z. Wang, Q. Huan, H. Wang, and K. Wang, A low loss platform for subwavelength terahertz graphene plasmon propagation, *Optical Materials* **128**, 112436 (2022).
- [68] N.I. Petrov, Propagation of Terahertz surface plasmon polaritons in a dielectric fiber with a metal wire core, *Fibers* **10**, 89 (2022).
- [69] X. Qin, Y. He, W. Sun, P. Fu, S. Wang, Z. Zhou, and Y. Li, Stepped waveguide metamaterials as low-loss effective replica of surface plasmon polaritons, *Nanophotonics* **12**(7), 1285 (2023).